AGU PUBLICATIONS

JGR

Journal of Geophysical Research: Oceans

RESEARCH ARTICLE

10.1002/2013JC009559

On the temporal memory of coastal upwelling off NW Africa

Aïssa Benazzouz[1,2], Josep L. Pelegrí[3], Herve Demarcq[4], Francisco Machín[5], Evan Mason[6], Abdellatif Orbi[1], Jesus Peña-Izquierdo[3], and Mordane Soumia[2]

[1]Institut National de Recherche Halieutique, Casablanca, Morocco, [2]Faculté des Sciences Ben M'Sik, Casablanca, Morocco, [3]Institut de Ciències del Mar, CSIC, Barcelona, Spain, [4]Institut de Recherche pour le Développement, Montpellier, France, [5]InvestigAdHoc, Telde, Spain, [6]Institut Mediterrani d'Estudis Avançats (IMEDEA UIB-CSIC), Esporles, Spain

Key Points:

- Coastal upwelling is observed to have seasonal temporal memory
- The coastal jet helps maintaining the structure of coastal upwelling
- A time-cumulative upwelling index is defined

Supporting Information:

- Supplementary figures

Correspondence to:
J. L. Pelegrí,
pelegri@icm.csic.es

Citation:
Benazzouz, A., J. L. Pelegrí, H. Demarcq, F. Machín, E. Mason, A. Orbi, J. Peña-Izquierdo, and M. Soumia (2014), On the temporal memory of coastal upwelling off NW Africa, *J. Geophys. Res. Oceans*, *119*, 6356–6380, doi:10.1002/2013JC009559.

Received 30 OCT 2013
Accepted 24 AUG 2014
Accepted article online 30 AUG 2014
Published online 22 SEP 2014

Abstract We use a combination of satellite, in situ, and numerical data to provide a comprehensive view of the seasonal coastal upwelling cycle off NW Africa in terms of both wind forcing and sea surface temperature (SST) response. Wind forcing is expressed in terms of both instantaneous (local) and time-integrated (nonlocal) indices, and the ocean response is expressed as the SST difference between coastal and offshore waters. The classical local index, the cross-shore Ekman transport, reproduces reasonably well the time-latitude distribution of SST differences but with significant time lags at latitudes higher than Cape Blanc. Two nonlocal indices are examined. One of them, a cumulative index calculated as the backward averaged Ekman transport that provides the highest correlation with SST differences, reproduces well the timing of the SST differences at all latitudes (except near Cape Blanc). The corresponding time lags are close to zero south of Cape Blanc and range between 2 and 4 months at latitudes between Cape Blanc and the southern Gulf of Cadiz. The results are interpreted based on calculations of spatial and temporal auto and cross correlations for wind forcing and SST differences. At temporal scales of 2–3 weeks, the alongshore advection of alongshore momentum compensates for interfacial friction, allowing the upwelling jet and associated frontal system to remain active. We conclude that the coastal jet plays a key role in maintaining the structure of coastal upwelling, even at times of relaxed winds, by introducing a seasonal memory to the system in accordance with the atmospheric-forcing annual cycle.

1. Introduction

The relevance of fisheries off NW Africa during the 1970s led to a systematic study of the region's upwelling characteristics [*Wooster et al.*, 1976; *Speth et al.*, 1978; *Hempel*, 1982; *Mittelstaedt*, 1983, 1991], although it was the routine availability of satellite sea surface temperature (SST) images in the 1980s that eventually brought a much better knowledge of its temporal and spatial variability [*Van Camp et al.*, 1991; *Nykjaer and VanCamp*, 1994; *Hernández-Guerra and Nykjaer*, 1997]. The message that progressively arose from remote sensing, not only SST but also sea surface color [e.g., *Gabric et al.*, 1993; *Carr and Kearns*, 2003] and sea surface height [e.g., *Lazaro et al.*, 2005; *Sangrà et al.*, 2009], was the three-dimensional (3-D) character of coastal upwelling. It has become clear that the classical two-dimensional (2-D) vertical cell is a useful idealization to understand the basic wind-driven mechanism behind coastal upwelling [e.g., *Gill*, 1982; *Csanady*, 1982; *Lentz and Chapman*, 2004; *Estrade et al.*, 2008; *Marchesiello and Estrade*, 2010], but the real coastal ocean commonly displays very diverse and, often, unexpected behaviors.

Despite this important realization, there have been tenacious efforts to *locally* relate sea surface winds to SST response in coastal upwelling regions. The typical procedure is to build simple functions, named upwelling indices, for both atmospheric forcing and ocean response in terms of instantaneous local variables, with the expectation for them to bear a direct relation. The reasoning behind this approach is that, in the 2-D perspective, the surface coastal ocean (top 100–200 m) responds quite rapidly (time scales of a few days) to changes in local wind forcing [e.g., *Csanady*, 1977; *DeSzoeke and Richman*, 1981, 1984; *Samelson and DeSzoeke*, 1988; *Pelegrí and Richman*, 1993; *Choboter et al.*, 2011] as compared with the typical temporal coherence of the winds (of the order of 1–2 weeks). Therefore, the evolution of SST on monthly and longer time scales may be approximately viewed as a direct response to local wind forcing.

A very simple wind-induced coastal upwelling index was first proposed by *Bakun* [1973]. The alongshore sea-surface wind stress induces seaward Ekman transport which, in steady state, causes upwelling of (relatively cold) subsurface waters. In a 2-D coastal ocean, the stronger the alongshore surface winds the more intense the upwelling, and the greater the SST difference between the coast and the interior ocean. In early studies, the wind field was estimated using surface pressure fields, and SST differences were only available from relatively scarce ship observations [*Wooster et al*., 1976; *Speth et al*., 1978]. Later, surface winds became available from weather forecast models and SST from infrared satellite images [*Nykjaer and VanCamp*, 1994; *Demarcq and Faure*, 2000]. Most recently, both data sets come routinely from satellite measurements [e.g., *Marcello et al*., 2011; *Pardo et al*., 2011; *Castellanos et al*., 2013a, 2013b; *Benazzouz et al*., 2014].

The cross-shore Ekman transport (or Bakun) index has been a widely used tool, reflecting its adequacy for many coastal regions. Nevertheless, the several major assumptions behind this simple index warn us that it may fail in a number of circumstances. First, it assumes steady state, ignoring any transient after a wind pulse. Second, it also ignores the advection of upstream momentum; we will argue later that this is a poor assumption off NW Africa where there is temporal memory caused by the dynamic connection between adjacent areas. Third, it does not consider internal friction associated with the alongshore jet; this friction may occur in the form of mixing, which brings both mass and momentum to the surface layer, reducing the actual Ekman transport and setting a limit on the offshore propagation of the upwelling front and the velocity of the alongshore jet. Finally, it neglects horizontal pressure gradients, thereby removing any geostrophic contribution that may drive convergence or divergence in the upwelling region; the 3-D character of upwelling indeed tells us that this will often be an unrealistic assumption.

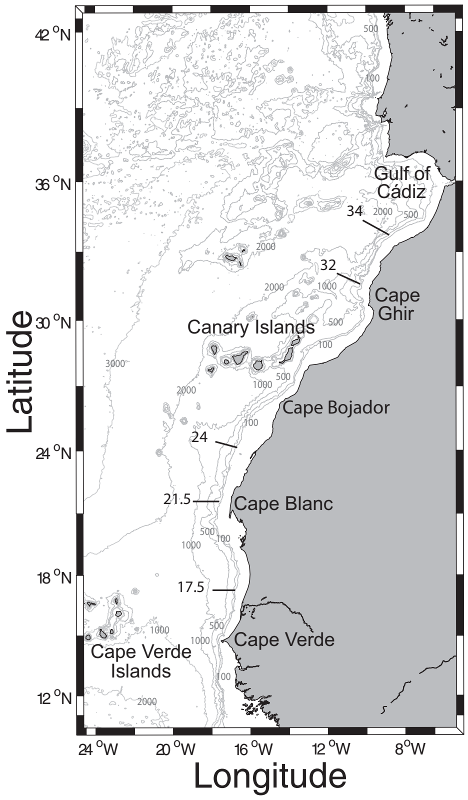

Figure 1. Region under study with some of the major geographic features; the isobaths shown are 100, 200, 500, 1000, 2000, 3000, and 4000 m. Five cross-shore sections used throughout the text are indicated.

The spatial and temporal coverage of contemporary satellite images has meant a revolution in our view of coastal upwelling, emphasizing the spatial and temporal variability of the coastal SST field and allowing us to examine the degree to which it is correlated with the surface wind field. It has progressively become evident that coastal upwelling depends not only on the intensity of the nearshore local winds, as the fundamental driving mechanism, but also on many other factors, mainly on the length and curvature of the coast, the bottom topography, the upstream flow, the neighboring interior ocean, and the temporal distributions of the wind field. Geomorphological factors do not change in time and could, in principle, be appraised by a position-dependent index that is (likely nonlinearly) related to the intensity of the wind. The temporal variability of the wind and the flow in the neighboring ocean, however, imply a non-Newtonian response of the coastal ocean, in the sense that it is not a direct function of the forcing but, rather, depends on the history of forcing over a region much larger than the area under consideration.

In this work, we focus on understanding how, at each location, the time history of forcing winds sets the intensity of coastal upwelling off NW Africa. The region of study goes from Cape Verde to the Strait of Gibraltar, or roughly between 15°N and 36°N, although in some descriptions we also include the adjacent areas (Figure 1). The area between Cape Blanc (about 21°N) and the southern Gulf of Cadiz (south of 36°N) has year-long upwelling-favorable winds, although north of the Canary Islands (located between 28°N and 29°N) the winds weaken substantially during winter [*Wooster et al*., 1976; *Nykjaer and VanCamp*, 1994;

Hernández-Guerra and Nykjaer, 1997; *Barton*, 1998]. Between Cape Verde (about 15°N) and Cape Blanc, the winds change with the season, being upwelling favorable only from late fall to late spring when they oppose the northward flowing Mauritania Current [*Nykjaer and VanCamp*, 1994; *Hernández-Guerra and Nykjaer*, 1997; *Demarcq and Faure*, 2000; *Lazaro et al.*, 2005; *Peña-Izquierdo et al.*, 2012; *Castellanos et al.*, 2013b]. Near Cape Blanc, we find an area dominated by intense coastal convergence and offshore export of coastal waters, typically not related to the local wind regime [*Pastor et al.*, 2008; *Peña-Izquierdo et al.*, 2012; *Castellanos et al.*, 2013b].

The north-easterly winds not only drive the coastal SST through upwelling but are also responsible for inducing the coastal baroclinic upwelling jet. This jet develops in the coastal transition zone (CTZ), located between the shelf and interior oceans [*Barton*, 1998], and enables communication between adjacent latitudinal upwelling regions. In some locations, the alongshore jet feeds/leaks from/to the interior eastern boundary ocean: input takes place between the Strait of Gibraltar and Cape Ghir, as the presence of the Strait breaks down the possibility of upstream flow [*Pelegrí et al.*, 2005a, 2006; *Mason et al.*, 2011, 2012; *Laiz et al.*, 2012], and output occurs at the Cape Verde frontal zone (CVFZ), where the subtropical upwelled waters are diverted offshore as they encounter tropical waters from the south [*Pastor et al.*, 2008; *Peña-Izquierdo et al.*, 2012]. The jet constitutes the actual boundary condition of the subtropical gyre; it can be considered as the easternmost branch of the southward Canary Current, and has been named the Canary Upwelling Current (CUC) [*Pelegrí et al.*, 2006].

For our analysis, we use a combination of climatological [*Troupin et al.*, 2010], satellite, and numerical model [*Mason et al.*, 2011] data. In particular, we expect the high-resolution numerical model to be informative about major local deviations from 2-D behavior. We also look at in situ data from years 2007 and 2008, including two extensive cruises, in order to gain a perspective on intraannual variability at short time scales. We use two nonlocal indices to understand how the upwelling system, characterized by SST difference between offshore and coastal waters, responds to the temporal memory of the alongshore wind stress. These indices are the wind-impulse anomalies, here understood as cumulative deviations from the mean upwelling conditions, and the time-lagged cumulative wind, defined as the time integral over a certain lag period such that it provides the highest correlation with the SST differences. The indices represent complementary views of the intensity of upwelling as compared with the classical Ekman upwelling index.

The paper is structured as follows. In section 2, we present the data sources. In section 3, we use climatological in situ and numerical data to discuss the seasonal cycle in the eastern boundary ocean and coastal upwelling region. Next, we focus on the skill of local indices to describe the seasonal cycle (section 4) and search for explanations of the nonlocal behavior (section 5). In section 6, we propose two indices which incorporate temporal memory and examine their behavior over the seasonal cycle. In section 7, we look at how all these indices perform for two individual years. We end with some concluding remarks (section 8).

2. Data Sets

2.1. In Situ Data

Our principal source of in situ data comes from the North-East Atlantic high-resolution (0.1° horizontal resolution on 33 depth levels) monthly climatology, produced by *Troupin et al.* [2010] using data-interpolating variational analysis (DIVA). The methodology takes into consideration both bottom topography and the coastline, allowing an improved description of the coastal areas.

We also use results from cruises carried out in November 2007 (29 October to 20 November, R/V García del Cid) and November 2008 (3–29 November, R/V Sarmiento de Gamboa). These cruises had excellent coverage of the continental slope between Cape Verde and the Strait of Gibraltar, with 150–200 km cross-shore sections about every degree of latitude [*Pastor et al.*, 2012; *Peña-Izquierdo et al.*, 2012]. Each section contains between five and ten stations, separated by distances of about 5 km nearshore and 30 km beyond the continental slope.

In our description, we focus on five sections at nominal latitudes of 17.5°N, 21.5°N, 24°N, 32°N, and 34°N. All sections, except the one at 17.5°N, are within the quasi-permanent upwelling region; for the two northern sections (32°N and 34°N), upwelling weakens substantially from late fall to late spring while the southernmost section (17.5°N) belongs to an area where upwelling ceases between late spring and late fall.

2.2. Numerical Data

The numerical data come from an extensively validated, high-resolution, Regional Oceanic Modeling System (ROMS) for the North-East subtropical Atlantic Ocean [*Shchepetkin and McWilliams*, 2005; *Mason et al*., 2011]. The model runs in sigma coordinates with a horizontal resolution of 7.5 km and 32 vertical levels, covering from 8°N to 50°N and from the coastline to 50°W. The model is integrated over 50 years with climatological atmospheric fields; in particular, the 0.25° resolution surface wind stress comes from the monthly 8 year Scatterometer Climatology of Ocean Winds (SCOW), which is based on QuikSCAT data between 1999 and 2007 [*Risien and Chelton*, 2008]. In this study, we have used years 11–50 of the numerical outputs, where each variable is a 3 day average; the analyses and figures presented are based on the averages calculated from these 40 years of output data.

2.3. Remote Sensing Data

SST data have been gathered by the Advanced Very High Resolution Radiometer (AVHRR) sensors of the National Oceanic and Atmospheric Administration (NOAA) satellite series. The 8 day AVHRR ascending mode SST data, with a resolution of about 5 km, are downloaded from the Physical Oceanography Distributed Active Archive Center of the National Aeronautics and Space Administration (NASA) (http://poet.jpl.nasa.gov/). We use 29 years of AVHRR data, from September 1981 to December 2009, to obtain the monthly climatology. Additionally, we examine data from January 2007 to December 2008 in order to appreciate the variability during a period that included extensive sampling off NW Africa.

Wind data are available from two different sources. The first set of data comes from the QuikSCAT sensor, available from the Center for Satellite Exploitation and Research at the Institut Français de Recherche pour l'Exploitation de la Mer (http://cersat.ifremer.fr). One product from this data set is the daily sea-surface horizontal wind stress, with a 0.5° latitude-longitude resolution; the corresponding climatology is obtained using the complete set of measurements (just over 10 years, from June 1999 to November 2009). The second data set corresponds to the Cross-Calibrated, Multi-Platform Ocean Surface Wind Velocity (CCMP) product, funded under the NASA Earth Science Enterprise, which combines wind measurements derived from scatterometer and microwave sensors by using a variational analysis method [*Atlas et al*., 2011]. A high spatial (25 km) and temporal (daily) record of ocean surface winds, available from July 1987 to December 2011, is also used to obtain the corresponding wind climatology (http://podaac.jpl.nasa.gov).

Both QuikSCAT and CCMP products have been explored to appraise the annual wind cycle over the region of interest and, in particular, to examine its relation with SST variability during years 2007 and 2008, when the two hydrographic cruises were carried out. A comparison of the wind fields from both products illustrates remarkable similarities, with analogous spatial and temporal patterns but slightly greater magnitude (of the order of 10%) for QuikSCAT. For the calculations in this paper, we use only the CCMP product.

3. The Coastal Upwelling Seasonal Cycle

The upwelling-favorable winds off NW Africa are associated with the anticyclonic motion of the lower atmosphere around the Azores High in the North Atlantic Ocean. The Azores High has a seasonal latitudinal motion, between about 25°N in late winter and 35°N in late summer, which drives the intensity and latitudinal extension of the north-easterly winds off NW Africa. Several coastal upwelling studies have looked at the predominant seasonal cycle in both wind forcing and coastal ocean response [*Wooster et al*., 1976; *Speth et al*., 1978; *Nykjaer and VanCamp*, 1994]. Time averaging over many years removes the synoptic variability in the atmospheric and ocean variables, which is equivalent to removing the short-scale (few days) ocean and atmospheric dynamics. Since the surface winds and upper ocean are tightly linked at these short scales, we could expect that such a low-pass filter would lead to a poor correlation between surface winds and SST; however, the correlation remains high, with the ocean lagging the atmosphere typically by about 1 month [*Nykjaer and VanCamp*, 1994].

Based on the local upwelling regime, we may divide the region of study into three areas separated by two confluence zones. These areas are located between Cape Verde and Cape Blanc (characterized by section 17.5°N), between Cape Blanc and the Canary Islands (represented by section 24°N), and between the Canary Islands and the Strait of Gibraltar (here illustrated by section 32°N); the two confluence zones correspond to the Canary Islands and the CVFZ. Figure 2 presents the seasonal cycle in the alongshore winds,

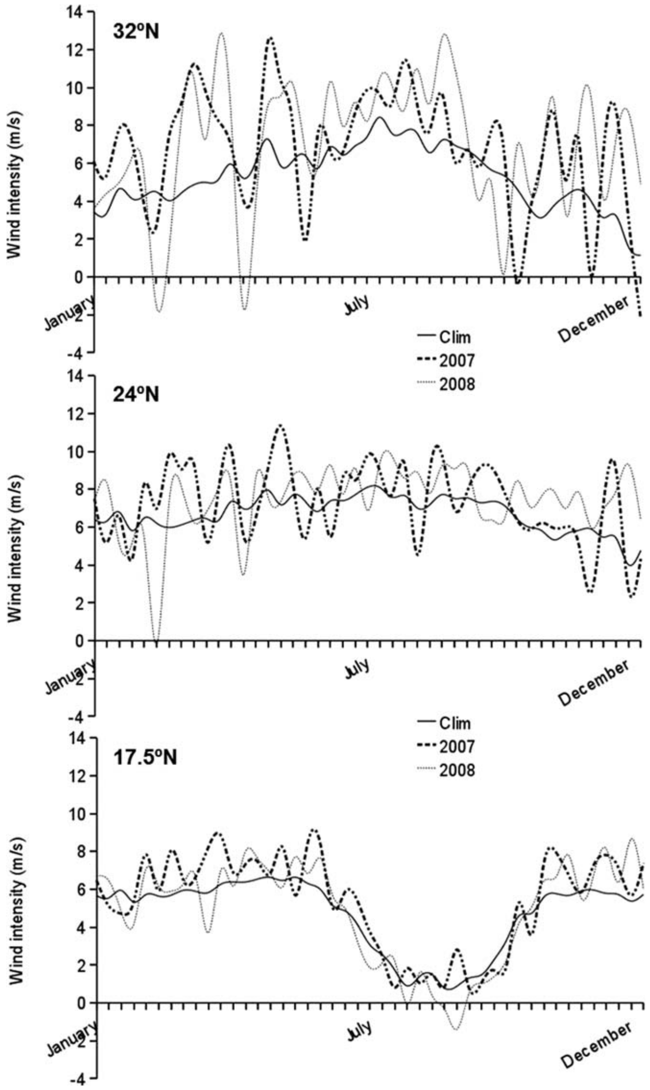

Figure 2. Seasonal variation of the alongshore mean wind (solid lines), and the corresponding values for 2007 (dashed lines) and 2008 (dotted lines), at three different latitudes: (bottom) 17.5°N, (middle) 24°N, and (top) 32°N. The values (m s^{-1}) correspond to a zonal average over 200 km adjacent to the African coastline.

averaged over 200 km adjacent to the continent, at latitudes characteristic of the three areas; the cycle is shown at 8 day intervals for the averaged year (from July 1987 to December 2011) as well as for two individual years (2007 and 2008). The whole region is favorable to upwelling all year long, except the southern area during summer and fall. The central area experiences relatively constant wind conditions throughout the year, and in the northern area the winds reach maximum values in summer and minimum values in late fall and early winter. The individual years illustrate the intermittency of the north-easterly winds, as they typically intensify on time scales of 1 week over different coastal areas, with simultaneous maximum values at adjacent areas in only a few instances. The temporal intermittency is of relatively small magnitude at 17.5°N and 24°N, but much greater at 32°N.

We next explore the seasonal variability of the eastern North Atlantic using the *Troupin et al*. [2010] in situ climatology and the *Mason et al*. [2011] climatological model output, both with horizontal resolution better than 10 km. Our objective is twofold: to examine whether the available spatial resolution is adequate to resolve the seasonal cycle of coastal upwelling and to investigate the existence of seasonality in the connections between the coastal ocean and the large-scale dynamics of the interior ocean [*Pelegrí et al*., 2005a, 2006; *Mason et al*., 2011].

The in situ climatological temperature fields at 0, 100, and 200 m depths are illustrative of the seasonal variability over the whole eastern boundary basin and, in particular, the coastal upwelling region (Figure 3). The offshore surface temperature fields change as a result of the air-sea heat exchange seasonal cycle, with maximum values in late summer. The 100 and 200 m levels are located below the surface mixed layer, except in February when the ocean surface layer deepens and releases its seasonal heat content [*Ratsimandresy et al*., 2001], and are therefore useful indicators of possible changes in the size and location of the subtropical gyre. The temperature fields at these levels do not, however, display remarkable changes except for a summer and, in particular, a fall increase in the CTZ between Cape Blanc and the Canary Islands. This change in the coastal pattern is coherent with the late summer and fall offshore diversion of the CUC at Cape Ghir and its northward fall recirculation near the African coast [*Pelegrí et al*., 2005a, 2006; *Machín et al*., 2006; *Mason et al*., 2011; *Laiz et al*., 2012].

The topography of the isotherms located immediately below the surface mixed layer (17, 16, and 15°C) confirms the extension of the subtropical gyre until the CVFZ and also endorses the possibility of a fall reversal in

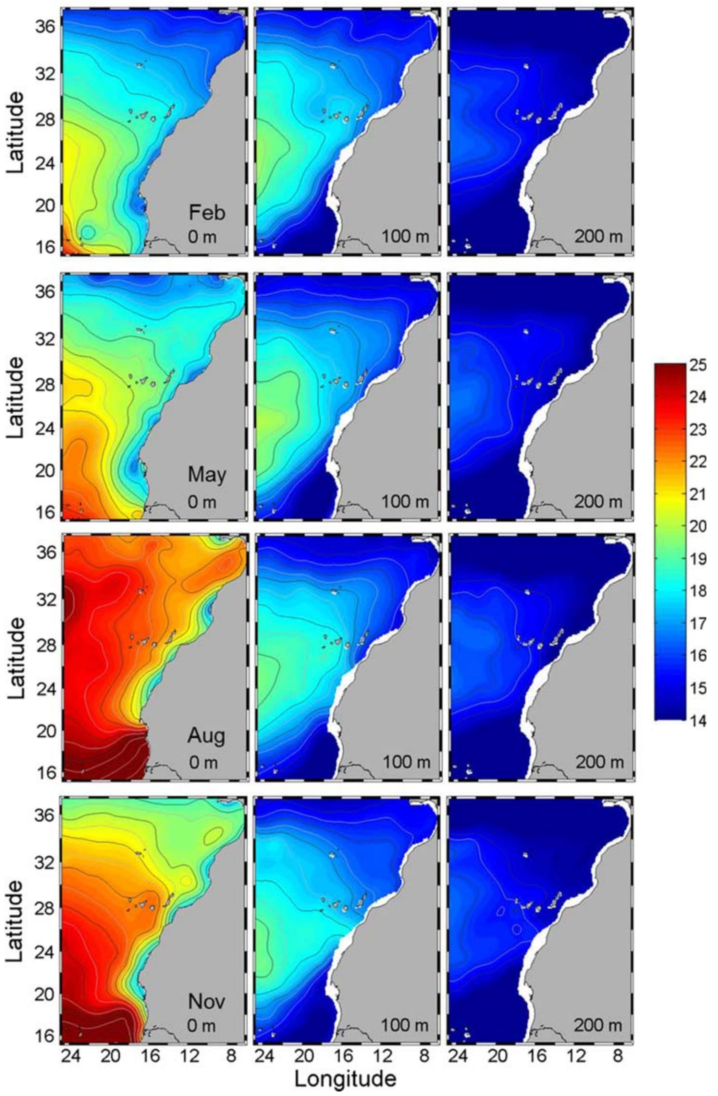

Figure 3. Temperature maps (°C) at (from left to right) 0, 100, and 200 m during (from top to bottom) February, May, August, and November, as deduced from the *Troupin et al*. [2010] climatology.

the CUC south of the Canary Islands (supporting information Figure S1). Additionally, the topography of the isotherms illustrates the north-eastward extension of the subtropical gyre during spring. As a result, the Canary Current approaches the continent north of the Canary Islands before turning south, leading to the observed northern intensification of the CUC [*Machín et al*., 2006; *Laiz et al*., 2012].

The temperature fields at different levels and the temperature topographies are particularly helpful for identifying the horizontal and vertical extension of coastal upwelling. The 15°C isotherm, which denotes the deepest level affected by upwelling (Figure 3), does not reach deeper than some 200 m in the CTZ (supporting information Figure S1). The surface temperature field is a good indicator of the fall and winter extension of upwelling south of Cape Verde, while the 17 and 16°C isotherms are most useful to describe its spring and summer northward expansion.

We may look at individual cross-shore sections (17.5°N, 21.5°N, 24°N, 32°N, and 34°N) to appreciate the temporal evolution of the mean temperature fields in the CTZ (supporting information Figure S2). The 21.5°N and 24°N sections display substantial upwelling all year long. Upwelling is intense down to some 250 m and is still discernible at 400 m. The 32°N section also shows considerable deep upwelling during May and August; upwelling remains appreciable in the top 100 m in November and disappears in February. The southernmost section (17.5°N) also presents upwelling during November, February, and May but reaching down to less than 100 m. The northernmost section (34°N), in contrast, only shows very weak upwelling in summer and fall.

The model climatological fields, as obtained with the *Mason et al*. [2011] model, are remarkably similar to the observations. For illustration, in Figure S3 (supporting information), we present the results for November. The surface, 100 and 200 m modeled temperature fields display very similar patterns to the in situ climatology (supporting information Figure S3, top). The only noticeable differences are a more intense Cape Ghir filament, in agreement with fall observations by *Pelegrí et al*. [2005b], and a narrower upwelling band in the Cape Blanc area. Similarly, the cross-shore sections at 17.5°N, 21.5°N, 24°N, 32°N, and 34°N display temperature fields that are very similar to the observations (supporting information Figure S3, bottom); some divergence from the in situ climatology is visible at 34°N where the model suggests the existence of a rather narrow and intense upwelling zone.

4. Local Indices

As briefly discussed in the Introduction, a 2-D coastal ocean (in the cross-shore vertical plane) would respond quite rapidly to upwelling-favorable winds, typically on the order of a few days. Because of this rapid adjustment, the implicit classical assumption has been that a local index for wind forcing should also be indicative of the ocean response. In this section, we examine the adequacy of this assumption for the seasonal cycle. The seasonal cycle is the major signal of variability and can be used to identify those times and locations where upwelling is expected to be most intense. But it is also during the seasonal cycle where we expect the major discrepancies between atmospheric forcing and ocean response: the seasonal cycle averages out the short-term response, which is the most direct atmosphere-ocean interaction, but retains the response associated with regional-scale interactions.

4.1. Definitions

The classical atmospheric forcing variable is the Ekman-upwelling, or Bakun, index [*Bakun*, 1973]. Under the assumption of an alongshore balance between Coriolis force and alongshore wind stress, the offshore Ekman transport per unit length (U, in the x direction) is given by:

$$U=\frac{\tau_{sy}}{\rho f}, \tag{1}$$

where τ_{sy} is the alongshore (in the y direction) surface wind stress, ρ is the surface water density, and f is the Coriolis parameter. The surface coastal winds are a function of latitude, calculated as the average wind value within 200 km of the coast. The surface stress vector is computed from the surface wind speed using the *Trenberth et al.* [1990] formulation, and the stress vector is then decomposed into components parallel (τ_{sy}) and perpendicular to the coast, where the coastal orientation is taken to be given by the mean direction of the 200 m isobath over a distance of 80 km. A characteristic stress of 0.1 N m^{-2} leads to a cross-shore transport (per unit length) of about 1 m^2 s^{-1} and, for a surface-mixed layer of depth $d=50$ m, to a cross-shore velocity of 0.02 m s^{-1}.

Notice that equation (1) assumes steady state and entirely neglects the advective terms, internal friction, and spatial pressure gradients [*Ekman*, 1905]. *Marchesiello and Estrade* [2010] proposed a modified index, which included the contribution from cross-shore geostrophic divergence resulting from alongshore pressure gradients.

Similarly, the ocean response has been classically expressed in terms of an SST difference index, calculated as the difference in temperature between upwelled waters over the shelf ($T_{\min}$) and waters further offshore ($T_{\max}$) [*Nykjaer and VanCamp*, 1994]:

$$\Delta T=T_{\max}-T_{\min}. \tag{2}$$

The minimum temperature is not very sensitive to the actual selection of the thickness of the coastal band but the maximum temperature depends more critically on the specified offshore search distance. This search distance has varied between 500 and 2000 km among different studies [*Nykjaer and VanCamp*, 1994; *Santos et al.*, 2005; *Benazzouz et al.*, 2006; *Marcello et al.*, 2011; *Castellanos et al.*, 2013b]; in particular, *Benazzouz et al.* [2014] choose $T_{\max}$ to be a function of time and latitude, selected such that it leads to the highest correlation between the SST difference and the Bakun index. *Santos et al.* [2005] showed the maximum temperature to not be very sensitive to a search distance that ranges between 400 and 1000 km. *Benazzouz et al.*'s [2014] best results, on the other hand, correspond to much larger distances, typically ranging between 1000 and 2000 km but reaching even further offshore at some latitudes.

Here we aim to choose a distance long enough to ensure that water parcels have enough time to fully warm as they move seaward after upwelling. However, we do not want it too large so that water parcels cannot be traced back to their nearshore origin. A simple estimate may be obtained by considering how upwelled waters warm as they move offshore [*Castellanos et al.*, 2013a, and references therein]. Off NW Africa, the net rate of heating per unit area Q ranges between moderate winter (20 W m^{-2}) and large summer (160 W m^{-2}) values. The corresponding heat flux per unit volume, q, is estimated by dividing these values by the depth of surface mixed layer, i.e., $q\equiv Q/d\equiv De/Dt=\rho c_p(D\theta/Dt)$, where e is the internal energy per unit volume, c_p is the specific heat (about 4000 J kg^{-1} K^{-1}), θ is potential temperature, and D/Dt refers to the material derivative. Discretizing and rearranging leads to the following expression

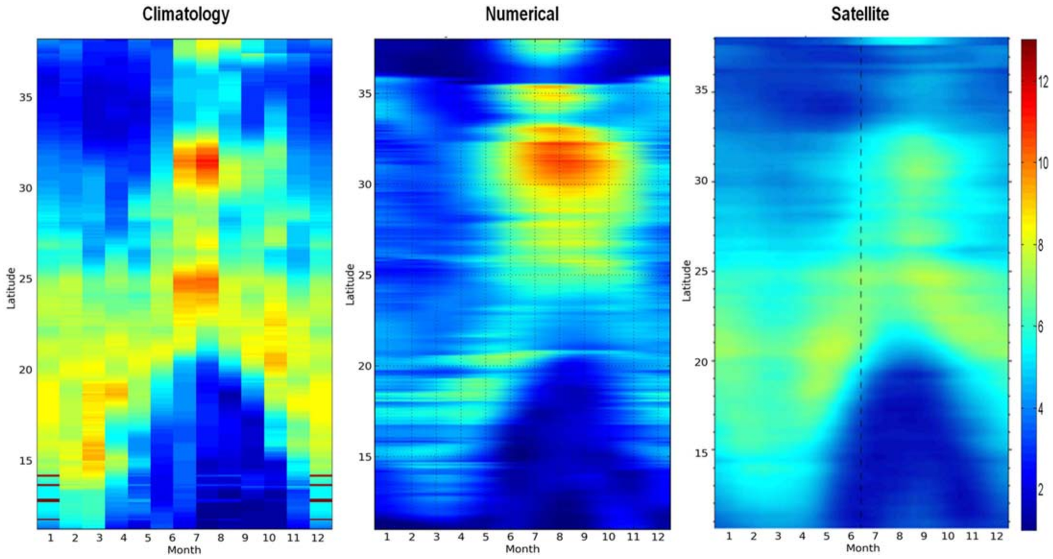

Figure 4. Time-latitude plots of the SST difference index (°C) as obtained (left) from the *Troupin et al.* [2010] climatology, (middle) with the ROMS model, and (right) from the time series average of 8 day AVHRR data.

for the required time increment: $\delta t = \rho c_p d\delta\theta/Q$; using the above values and $d = 50$ m, this expression gives $\delta t = A\delta\theta$, where the constant A ranges between about 10^6 and 10^7 s K^{-1} for summer and winter conditions, respectively. Therefore, the range of influence $\delta x = u\delta t$ is proportional to the speed u at which the water parcel is advected seaward and to the temperature increase of the water parcel (the temperature difference, approximately zonal, between the upwelled and offshore waters), i.e., $\delta x = uA\delta\theta$. For a moderate velocity of 0.02 m s^{-1} and a temperature difference of about 5°C, this expression gives δx between 100 and 1000 km (summer and winter, respectively).

This above brief discussion shows that determining T_{max} is not a trivial issue but, in any case, the offshore distance should not be less than about 1000 km. Further, it is clearly preferable to have a small error caused by an excessively long distance, related to the relatively small far-offshore SST zonal gradients, than a potentially large error associated with an excessively small search distance. In some instances, for example, the frontal upwelling system may be located quite far offshore, up to several hundred kilometers from the coast [*Peña-Izquierdo et al.*, 2012]. Therefore, in this work, we have computed the maximum zonal temperature using a search distance of 2000 km.

The SST difference index was normalized by *Demarcq and Faure* [2000] to account for the fact that maximum temperature differences depend not only on the offshore surface temperature but also on the subsurface temperature. Their modification, however, requires knowledge of coastal temperatures, for each latitude and time of the year, at the maximum depth of wind influence. *Benazzouz et al.* [2014] have estimated these to correspond to the lowest SST values at the coast, as sampled by the AVHRR between 1981 and 2011.

4.2. Time-Latitude Distributions

We construct the SST difference index from the in situ climatological data (going as far back as the 1950s although mostly gathered since the 1980s), the numerical climatological simulation (averages of 40 year output, forced by a monthly climatological year obtained with wind data from 1999 to 2007) or the satellite AVHRR data (1981–2009 period). The results, presented as latitude-time plots, display remarkably similar patterns but with somewhat different intensities (Figure 4). The plots clearly show the existence of three distinct areas: upwelling shows high seasonality between 11°N and 21°N and between 26°N and 35°N, and remains intense all year long between 20°N and 26°N. At high latitudes (26°N–35°N), upwelling becomes intensified in summer and fall and weakens, but does not quite disappear, in winter and spring. At low latitudes (11°N–21°N), it completely disappears during several months; centered around August, the lower the latitude the longer the period without upwelling. South of the Canary Islands, the largest and smallest values, respectively, show up on the in situ and numerical climatology. Between the Canary Islands and the

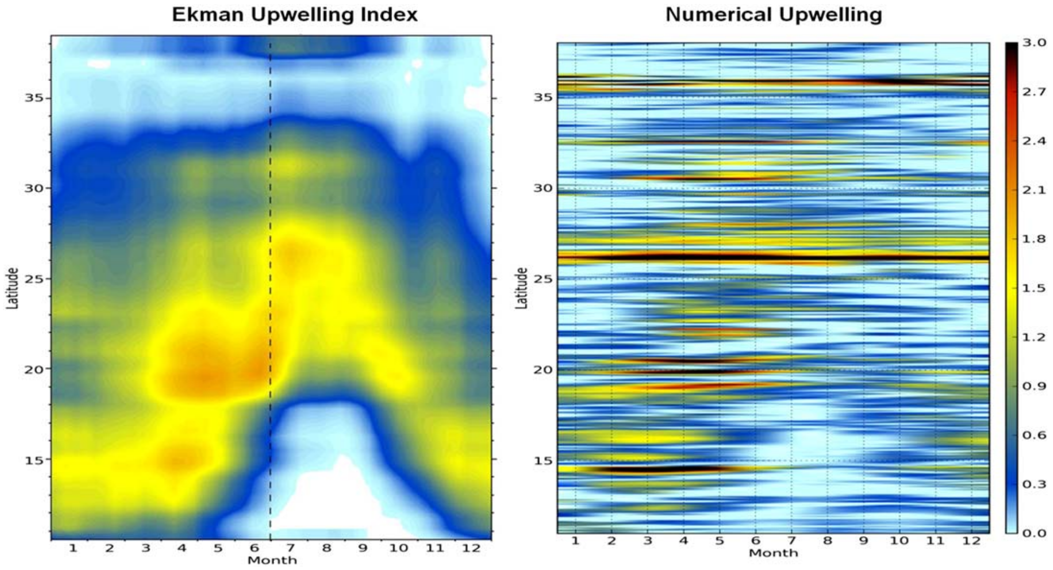

Figure 5. Time-latitude plots of (left) the cross-shore Ekman upwelling index ($m^2 s^{-1}$) and (right) the zonally integrated coastal vertical velocity obtained with the ROMS model, as described in the text ($m^2 s^{-1}$).

Strait of Gibraltar, the largest and smallest values correspond to the numerical and satellite data, respectively.

The numerical monthly climatology, with spatial resolution of 7.5 km, is very instructive (Figure 4, middle). The plot shows high spatial intermittency at the mesoscale and submesoscale with substantial temporal coherence, where thin bands of intensified upwelling last for several months. *Mason et al*. [2012] have already reported the existence of such high spatial variability north of the Canary Islands but it is very striking that it remains even when averaged over 40 years of numerical output, indicating that upwelling is strongly modulated by the coastal geomorphology. The satellite climatology (5 km and 8 days resolution) also illustrates the presence of spatial intermittency and temporal coherence, yet is less sharp than in the numerical fields (Figure 4, right); the agreement between the satellite and numerical patterns is remarkable. Finally, the in situ climatology has very good latitudinal resolution (0.1°) but low (1 month) temporal resolution (Figure 4, left), resulting in a signal which changes smoothly in space and is piecewise in time. Despite the high spatial resolution, and in contrast with the numerical data, it is clear that there is little or no spatial intermittency. This is undoubtedly caused by the relatively long correlation scale, typically several degrees, used to generate the climatology [*Troupin et al*., 2010].

The observations of SST difference may be compared with the offshore Ekman transport (per unit length, equation (1)) as the simplest local index for wind forcing (Figure 5, left). The comparison shows that wind forcing and SST response do exhibit a similar pattern, but there are two main discrepancies. First, the maximum SST differences north of Cape Blanc (21°N) are delayed with respect to Ekman transport. Second, the Ekman-transport index predicts highest spring upwelling values between 18°N and 24°N, which are not reflected in the SST differences. The disparities likely respond to the simplifications behind the Ekman-transport formulation, such as the omission of any temporal memory related to the upstream flow conditions.

Figure 5 (right) shows the actual climatological upwelling as inferred from the numerical model. Upwelling is calculated from the vertical velocities immediately below the depth of the surface mixed layer, integrated offshore from the coast so that we have vertical transport per unit length of the coastline (units of $m^2 s^{-1}$). We follow the procedure described in *Mason et al*. [2012], so integration is terminated when upwelling remains low for a sufficiently long distance (here respectively taken as 1.3 m d^{-1} and 130 km). The integrated transports are plotted in the 0–3 $m^2 s^{-1}$ interval although these limits are greatly exceeded in some locations (up to a factor of 100). Values less than zero are very rare except near the Strait of Gibraltar; in contrast, values larger than 3 $m^2 s^{-1}$ are common (black areas in Figure 5, right).

The time-latitude pattern of upwelling (Figure 5, right) has the same long temporal coherence and high spatial intermittency as the model SST-difference index (Figure 4, middle); they also share the same gross shape

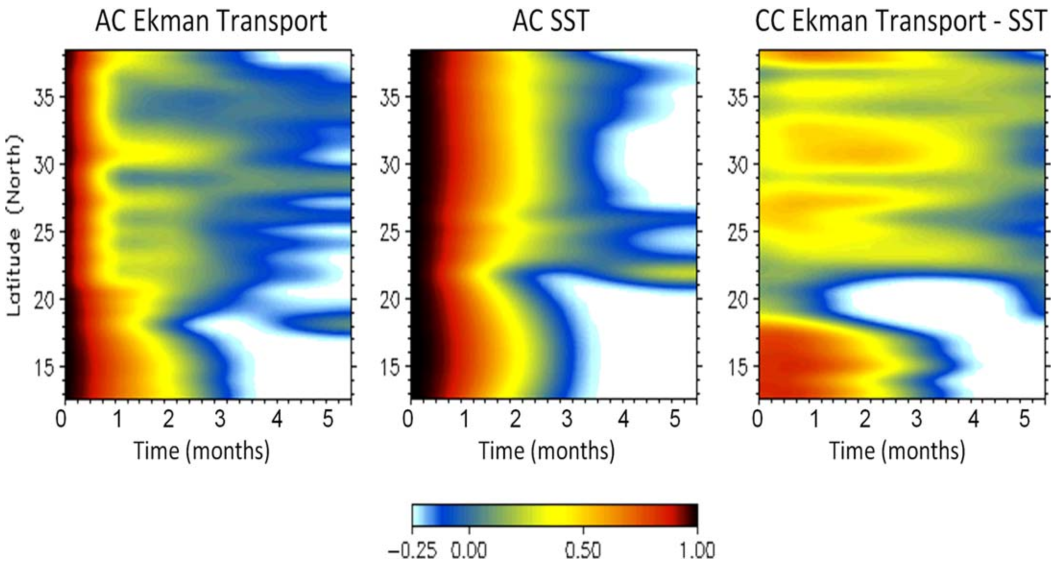

Figure 6. Temporal correlation as a function of latitude: (left) autocorrelation of the Ekman transport, (middle) autocorrelation of the SST difference, and (right) cross correlation between Ekman transport and SST difference.

but with several noteworthy differences. One major difference is the year-long high upwelling patch found off and north of Cape Bojador (26°N–27°N), which does not show up in the SST difference. Also, the late-summer SST differences between 29°N and 33°N and at about 35°N are not reflected in the vertical transport. Further north, at about 36°N, the vertical transports reach maxima precisely where the SST differences drop to zero, probably related to the Mediterranean Water outflow.

5. Temporal and Spatial Memory of the Upwelling System

5.1. Temporal and Spatial Correlations

Both inertia and upstream conditions introduce temporal and spatial memory to the system. We are used to thinking of the upwelling system in terms of its inertia. The alongshore wind drives the alongshore coastal jet which, in turns, experiences internal friction that limits its growth. As the wind ceases or weakens, friction will progressively reduce the alongshore motion, the larger the momentum (greater inertia) the longer it will take to fully stop. It is the Coriolis force associated with the alongshore jet that induces the offshore motion. Because of the coastal constraint, this offshore motion creates a cross-shore pressure gradient which opposes the Coriolis force, eventually limiting the size of the cross-shore transport; the cross-shore motion will only decrease when the alongshore jet weakens.

The upstream flow, however, is equally important. The alongshore motion is influenced by the recent history of local forcing but it is also affected by what was taking place sometime before in the neighboring areas. As a consequence, the upwelling vertical structure will decrease only if the winds cease all along the coast for a sufficient amount of time. Some of these ideas were endorsed by *Gill and Clarke* [1974] when they stated that upwelling depends “not just on local forcing” but on the forcing that the flow experienced “at earlier times as it moved along the coast to the region under consideration.” *Gill and Clarke* [1974] were thinking about propagating waves but the same is true for the geostrophic coastal jet.

We may consider winds as acting over (dynamically connected) adjacent areas in such a way that their temporal intermittency, and their effect on the coastal ocean, is smoothed out. For this to be possible at one particular location, the temporal scale of the ocean response has to be longer than the temporal scale of the atmospheric forcing. The idea is that wind may locally relax but it does so over distances and times short enough for upwelling to be maintained over a much greater region thanks to the alongshore jet connection. To explore this possibility, we look at the temporal and spatial correlations for wind forcing and SST response; specifically, we calculate the autocorrelation of Ekman transport (proportional to the alongshore wind stress), the autocorrelation of SST difference, and the cross correlation between both variables (Figures 6–8).

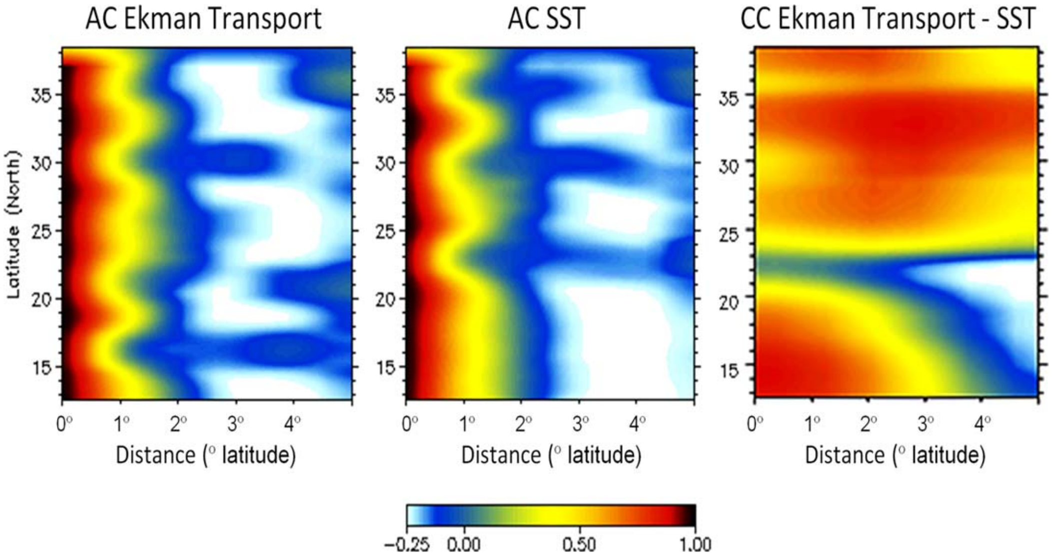

Figure 7. Annual-mean spatial correlations as a function of latitude: (left) autocorrelation of the Ekman transport, (middle) autocorrelation of the SST difference, and (right) cross correlation between Ekman transport and SST difference.

To calculate the correlations, we use the whole available time series, i.e., 29 years of AVHRR data for the SST differences and over 10 years of wind data for the Ekman transport. To calculate the temporal correlations, we set the latitude and work with the corresponding time series. To calculate the spatial correlations, we follow two steps. First, we set one latitude and time, and calculate the correlations using the data for that time over a latitudinal interval of 5°; for example, we may calculate the correlations at 24°N for the first week of

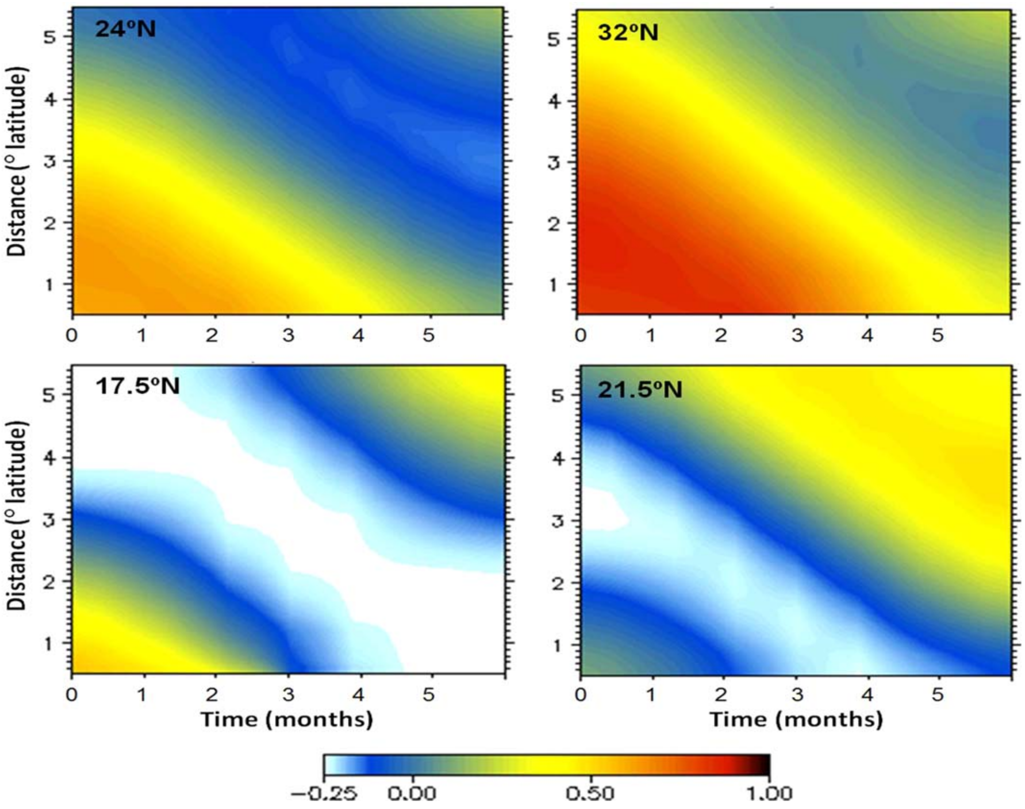

Figure 8. Time-distance cross correlations between Ekman transport and SST difference at selected latitudes: (bottom left) 17.5°N, (bottom right) 21.5°N, (top left) 24°N, and (top right) 32°N.

January 2009 between 21.5°N and 26.5°N. The second step is to repeat this calculation for different times and take the corresponding averages; for example, to obtain the January value we average over all weeks of January from the available time series, and to obtain the annual mean value we average over the whole time series.

The behavior of the temporal correlations off NW Africa confirms the existence of a southern area, from Cape Verde to Cape Blanc (15°N–21°N), where upwelling is seasonal, and a northern area, from north of Cape Blanc to near the strait of Gibraltar (22°N–35°N), where upwelling takes place all year long (Figure 6). Both areas are separated by the confluence zone between the subtropical and tropical gyres, located immediately north of Cape Blanc (21°N–22°N), at the origin of the Cape Blanc giant filament offshore extension. In the northern area, the wind autocorrelation is substantially shorter than the SST-difference autocorrelation, while in the southern area they are of similar size. If we choose a correlation threshold near 0.4 it turns out that the wind has a temporal memory of about 3 weeks and almost 2 months in the northern and southern areas, respectively (Figure 6, left). Using this same threshold, the SST difference has a temporal memory of about 2 months north of 22°N and slightly less in the southern area, with a minimum in the boundary between both areas (Figure 6, middle). The characteristic time scale obviously depends on the selection of the correlation threshold, being less sensitive when we select this threshold at the inflection point of the correlation distribution; under the common assumption of Gaussianity, this happens for correlations close to 0.4 [e.g., *Ruiz et al*., 2014].

The relatively long temporal ocean memory in the northern area, as compared with the atmospheric memory, suggests that in this area the coastal ocean is not solely driven by the winds. This result is confirmed by the cross correlation between Ekman transport and SST differences (Figure 6, right). In the northern area, the cross correlation has moderate maximum values for time lags as long as 3–4 months, i.e., for times longer than those that characterize both atmospheric forcing and ocean response. These moderate correlation values at long time scales may be interpreted as the observed response of a long-time and high-inertia upwelling system. The situation is quite different in the southern area, where the cross correlation is maximum at zero time lag and remains large for times of about 2 months, i.e., a time scale on the same order as those which characterize both the wind field (Figure 6, left) and the ocean response (Figure 6, middle). Finally, in the confluence between the northern and southern areas (near 22°N), the cross correlation remains low at all lag times.

The annual-mean spatial correlations complement the above picture (Figure 7); note that correlations are symmetric for positive and negative lags so in the following discussion the values in Figure 7 are doubled. Again choosing 0.4 as a threshold correlation value, the autocorrelations for both the annual-mean Ekman transport and SST differences are about 2° of latitude, or close to 200 km, over the whole region (Figure 7, left and middle). Local minima are found at latitudes associated with geomorphological features: 36°N (Strait of Gibraltar), 28°N–30°N (Canary Islands), and near 22°N (just north of Cape Blanc). In contrast, the cross correlations between Ekman transport and SST differences are much longer over most of the domain (between 4° and 6° south of Cape Blanc and longer than 7° north of Cape Blanc; Figure 7, right), again confirming the large-scale and high-inertia character of the upwelling system; it is only at the confluence of both the southern and northern areas (near about 22°N) that the cross correlation disappears at all lag distances. In summer and fall (not shown), the cross correlation breaks down at the latitude of, and immediately below, the Canary Islands, probably reflecting the existence of the anticyclonic circulation discussed in section 3; in winter (not shown), the correlation turns negative south of Cape Blanc; at times of intensified upwelling, indicating that the SST difference patterns come ahead of the winds.

A complementary view of the relevant spatial and temporal scales may be obtained by calculating the combined spatial-temporal cross correlations between Ekman transport and SST differences at selected latitudes (Figure 8); for this calculation, the spatial cross correlation is calculated by successively shifting the SST difference by one time interval (8 days). The results show the existence of bands with different values, consistent with the observed temporal and spatial cross correlations (Figures 6 and 7), that characterize the combined time-space memory at the selected latitudes.

The two different domains, south and north of Cape Blanc, are, respectively, characterized by relatively short and long spatial and temporal scales. In particular, north of Cape Blanc (here characterized by 24°N and 32°N), the two time series are correlated with temporal scales as large as 3 months and 7° (here again, as

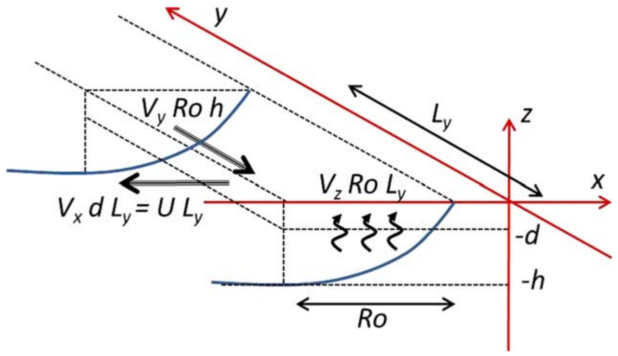

Figure 9. Schematics of the main elements controlling mass conservation in the coastal upwelling system.

for Figure 7, the spatial distances are doubled), therefore confirming the high temporal and spatial coherence of the upwelling frontal system. These figures also show that the northern region responds in phase, i.e., there is nothing like a maximum correlation at some upstream distance and earlier time, something to be expected if the region were characterized by the generation and downstream propagation of transient pulses (except possibly for propagating waves which, because of their very fast propagation speed, do not provide a mechanism for the persistence of upwelling at long time scales). Quite to the contrary, the confluence region (here illustrated by the 21.5°N section) exhibits a remarkable lack of correlation: it barely reaches the 0.4 threshold for long time and spatial lags (for example, 4 months and 4° of latitude). Such a lack of correlation suggests that the local dynamics off Cape Blanc are the result of the complex interaction between the quite distinct neighboring regions [*Peña-Izquierdo et al.*, 2012].

In the northern area, the wind-SST cross correlations are indicative of the upstream distance of influence: a time scale of 2 months (some 5×10^6 s) and a length scale of 7° (about 700 km) correspond to a velocity of 0.14 m s^{-1} (Figure 8, top). The alongshore upwelling jet is the necessary connection for the correlation to remain high over time scales longer than the intermittency of the wind, almost over one whole season. The conclusion is that the forcing winds set the intensity of coastal upwelling north of Cape Blanc in two different ways: directly, on time scales of the order of 1–2 weeks; indirectly, through the generation of the latitudinally coherent alongshore coastal jet, on time scales of the order of 1–3 months. South of Cape Blanc the situation is substantially different as the coastal upwelling jet is opposed by the Mauritania Current.

5.2. The Relevance of the Alongshore Jet

The momentum equations (retaining only the stress caused by the vertical shear) in the cross-shore (x, positive eastward) and alongshore (y, positive northward) directions are (Figure 9):

$$\frac{Du}{Dt} - fv = -\frac{1}{\rho}\frac{\partial p}{\partial x} + \frac{1}{\rho}\frac{\partial \tau_{zx}}{\partial z}, \tag{3}$$

$$\frac{Dv}{Dt} + fu = -\frac{1}{\rho}\frac{\partial p}{\partial y} + \frac{1}{\rho}\frac{\partial \tau_{zy}}{\partial z}, \tag{4}$$

where (u, v) are the velocities in the (x, y) directions, t is time, z is the vertical direction (positive upward), p is pressure, ρ is water density, $\left(\tau_{zx}, \tau_{zy}\right)$ are the (x, y) horizontal components of the stress on constant-depth levels, and $D/Dt \equiv \partial/\partial t + u\partial/\partial x + v\partial/\partial y$ refers to the material derivative.

In order to help visualize the principal physical mechanisms responsible for the maintenance of an upwelling system, we assume a two-layer structure with only the upper layer in motion (1.5 layer model) and vertically integrate the equations. The integrated equations for this active layer are

$$\frac{Du}{Dt} - fv = -g\frac{\delta\rho}{\rho}\frac{\partial h}{\partial x} + \frac{\left(\tau_{sx} - \tau_{bx}\right)}{\rho h}, \tag{5}$$

$$\frac{Dv}{Dt} + fu = -g\frac{\delta\rho}{\rho}\frac{\partial h}{\partial y} + \frac{\left(\tau_{sy} - \tau_{by}\right)}{\rho h}, \tag{6}$$

where the density and velocities now refer to the upper layer, $\delta\rho$ is the density difference between the lower and upper layers, g is the gravitational acceleration, and h is the depth of the upper layer; the s and b subindices refer to the sea surface and bottom of the upper layer, respectively.

In the cross-shore direction, for sufficiently long times and in the absence of substantial cross-shore winds, the momentum balance remains dominated by a baroclinic jet in geostrophic balance:

$$fv = g\frac{\delta\rho}{\rho}\frac{\partial h}{\partial x}. \tag{7}$$

This balance tells us that the baroclinic coastal-upwelling structure, reflected by the cross-shore SST differences, will hold as long as the alongshore jet remains active.

In order to understand the relative importance of the different forces controlling the time evolution of the alongshore jet, we turn to the alongshore momentum equation. The classical Ekman index assumes a balance between the Coriolis force associated with the cross-shore motion and the alongshore stress gradient, $fu = \tau_{sy}/\rho h$, which is precisely equation (1) with the definition $U = uh$. This relation ignores the acceleration, pressure gradients, and bottom frictional terms acting over the alongshore motion. *Marchesiello and Estrade* [2010] discussed how the alongshore pressure gradients may affect this balance. Off NW Africa these gradients may be locally related to the geomorphology of the coast or be caused by the seasonal buildup through large-scale winds; they can be viewed as a long-term rectification of the Coriolis force and will be ignored in the forthcoming discussion. Therefore, we are left with the following integrated equation:

$$\frac{\partial v}{\partial t} + u\frac{\partial v}{\partial x} + v\frac{\partial v}{\partial y} + fu = \frac{\left(\tau_{sy} - \tau_{by}\right)}{\rho h}. \tag{8}$$

The first consideration is to assess the potential role of internal friction, in the above equation represented simply by the interfacial friction between both layers, τ_{by}. This interfacial friction is commonly expressed as linearly proportional to the velocity difference between adjacent layers, i.e., $\tau_{by} = r\rho(v_1 - v_2)$, where the 1,2 subindices now, respectively, refer to the upper and lower layers; when the flow is over the sea bottom, the expression reduces to $\tau_{by} = r\rho v$, and the friction coefficient r has typical values of 10^{-3} m s^{-1} [*Csanady*, 1982; *Gill*, 1982; *Lee et al.*, 2001]. For the interfacial friction between adjacent vertical layers, however, the friction coefficient may change depending precisely on the rate of exchange of horizontal momentum deficit or excess between the adjacent layers. From this perspective, the relation acquires full physical meaning [*Geisler and Kraus*, 1969; *Pelegrí and Richman*, 1993]: $\tau_{by} = w_e\rho(v_1 - v_2)$, where w_e is the two-way vertical exchange between both layers.

It is important to realize that w_e is not the vertical velocity of the upwelling water, which would set the vertical displacement of the interface between the upper and lower layers, but rather the two-way vertical velocity through this interface. During the onset of upwelling, w_e is likely small but as the jet develops the flow approaches critical conditions and mixing (and hence friction) is greatly enhanced; once the wind relaxes, the upwelling system again diverts from the critical conditions and w_e decreases rapidly [*Kundu and Beardsley*, 1991; *Pelegrí and Richman*, 1993]. Following *Lee et al.* [2001] this exchange velocity may be parameterized as $w_e = (A_v f/2)^{1/2}$, where A_v is the vertical eddy viscosity coefficient. At times of critical conditions, A_v may well reach values as large as $10^{-3} - 10^{-2}$ m^2 s^{-1}, in contrast to background levels of $10^{-5} - 10^{-4}$ m^2 s^{-1} [*Peters et al.*, 1988]; the corresponding w_e values will therefore range between 10^{-4} m s^{-1} during the initial and decay upwelling phases and 10^{-3} m s^{-1} at times of intense upwelling-favorable winds.

Consider the case when the wind ceases and upwelling decays. In this circumstance, the cross-shore velocity becomes weak and, temporarily neglecting the alongshore advective term, the alongshore momentum equation reduces to

$$\frac{\partial v}{\partial t} \cong -\frac{w_e v}{h}, \tag{9}$$

This situation will correspond to weak vertical mixing velocities, $w_e \approx 10^{-4}$ m s^{-1}; considering an upper layer 150 m thick, the relevant time scale turns out to be $h/w_e \approx 17$ days. In the absence of advection, friction sets a local temporal memory of the upwelling system of the order of 2–3 weeks.

However, alongshore advection has the capacity to regulate such frictional decay. As shown above (equation (7)), the main requirement for the sustainment of the coastal upwelling frontal system is the local maintenance of the alongshore jet, i.e., $\partial v/\partial t \cong 0$. Therefore, when wind and upwelling cease, equation (8) may alternatively be simplified as (now keeping the alongshore advective term)

$$v\frac{\partial v}{\partial y}=-\frac{w_e v}{h}. \tag{10}$$

As explained before, the Ekman balance neglects the acceleration and frictional terms, implicitly assuming there is a limit in the development of the alongshore jet when acceleration and friction balance each other. However, our analysis of time and space correlations suggests that, on time scales from several weeks to a couple of months, the acceleration term Dv/Dt may be equally important in the alongshore balance. At times when the wind ceases, the structure of the coastal upwelling jet is maintained as long as the alongshore jet does not significantly decrease because of interfacial friction. Equation (10) shows that this is possible thanks to the acceleration, specifically through the alongshore advection of y momentum, $v\partial v/\partial y$.

If we set dimensional scales as $(x,y)=(L_x x', L_y y')$, $(u,v)=(V_x u', V_y v')$, $w_e=V_z w_e'$, and $t=Tt'=(L_y/V_y)t'$, it turns out that equation (10) implies $V_y h \approx V_z L_y$. Therefore, the key requirement for the maintenance of upwelling is an alongshore jet active over an upstream distance $L_y \approx V_y h/V_z$. Using characteristic values of 10^{-4} and 0.2 m s^{-1} for the vertical and alongshore velocities, respectively, we find an alongshore scale of 300 km. The alongshore velocity gradient does not need to be very sharp to sustain friction: an alongshore jet located 300 km upstream is sufficient to provide the required momentum. This distance is not much longer than the spatial correlation of both the surface winds and the SST differences in most of the upwelling region, of the order of 2° of latitude (Figure 7, left and middle), therefore sustaining the possibility that the upstream flow brings the required momentum. Alternatively, we may assess the time scale during which the alongshore jet can provide for the cross-shore Ekman flow. The characteristic time scale, estimated as $T=L_y/V_y \approx h/V_z$, turns out to be equal to the frictional decaying time scale, some 17 days. This value is similar to the temporal scale of the wind, as deduced from the temporal autocorrelation (Figure 6), suggesting that wind intermittency is not long enough to allow upwelling to fully relax, and bringing a long spatial cross correlation between atmospheric forcing and ocean response (Figure 7, right).

It is not enough, however, for the upstream flow to be large enough to sustain the cross-shore momentum balance; it also has to provide for the mass balance, as schematically shown in Figure 9. Notice that when turning equations (5) and (6) into equations (7) and (10), we could have invoked the coastal constraint to imply there is no momentum advection from shore; this is not the case when considering cross-shore water divergence, here the proper scale for the cross-shore velocity is the Ekman transport divided by the depth of the surface mixed layer. For the cross-shore flow to be approximately supplied by the alongshore jet, the equation of volume conservation is $\partial u/\partial x+\partial v/\partial y \approx 0$. This 2-D relation is to be integrated over a control volume encompassing the upwelling jet, with the alongshore transport supplied through the cross-section of the upwelling frontal system and most of the offshore transport taking place in the surface mixed layer. The resulting dimensional relation is $V_y h Ro \approx V_x d L_y = U L_y$, where h is the characteristic depth for the upwelling frontal system (mean depth of the upper layer), Ro is its width, d is the depth of the surface mixed layer, and U is the cross-shore Ekman transport (equation (1)). The width Ro is given by the internal Rossby radius of deformation, $Ro=(g'h)^{1/2}/f$, where $g'=g\delta\rho/\rho$; using $h=150$ m and $g'=3\times10^{-4}$ leads to $Ro=21$ km. The alongshelf scale becomes $L_y=(h/d)(V_y/V_x)Ro$; typically h/d is about 3 and V_y/V_x about 10, so $L_y \cong 30Ro$, or some 630 km. This long distance implies that the water transported by the alongshore jet is plenty to provide for the necessary offshore transport over a few degrees of latitude and yet maintain a significant alongshore load.

It is important to note that both above dimensional relations, $V_y h \approx V_z L_y$ and $V_y h Ro \approx V_x d L_y$, are actually a statement of continuity: for upwelling to be sustainable in the absence of alongshore winds, the offshore transport ($V_x d L_y$) has to be provided by the alongshore transport associated with the coastal upwelling jet ($V_y h Ro$) through vertical exchange over the whole upwelling frontal system ($V_z L_y Ro$) (Figure 9).

6. Nonlocal Indices

A local index depends only on the prevailing (both in time and space) forcing conditions; for upwelling, this essentially means the alongshore wind at the location under study. On the contrary, a nonlocal upwelling index requires some temporal and/or spatial memory of the previous atmospheric and oceanic conditions. The above discussion on the relevance of the upstream conditions indeed shows the convenience of using a nonlocal approach for a proper description of upwelling off NW Africa.

Any nonlocal index is meant to have greater predictive skill of the upwelling conditions but, unavoidably, this is done at the expense of simplicity, generally requiring some knowledge of the ocean response. In practice, however, this is greatly simplified because the adjacent regions off NW Africa are dynamically connected, i.e., upstream information is brought about by the alongstream coastal upwelling jet. This has two effects: filters the effect of wind intermittency on upwelling and converts a spatial lag into a temporal lag.

6.1. Definitions

Schwing et al. [2006] and *Pierce et al*. [2006] defined a cumulative index simply as the summation of the daily indices, based on the argument that it better represents the cumulative effect of upwelling on ecosystem functioning. Actually, the summation of daily indices is the time integral of the Ekman transport, or wind impulse, a quantity early defined by *Csanady* [1977] to assess the time needed for full upwelling to occur following wind set up.

To best appraise the significance of the wind impulse, consider a 2-D idealization. An upwelling steady state would be reached if a wind event remains constant long enough, this corresponding to a wind impulse that increases linearly in time. Contrarily, a changing wind will drive variations in the intensity of upwelling, resulting in a nonlinearly changing wind impulse. Under this perspective, in order to reflect the variability from the time-mean upwelling-favorable conditions, it is most convenient to define the wind-impulse anomaly [*Castellanos et al*., 2013b]. The procedure consists to adjust a linear fit to the wind impulse and to subtract the difference between the actual values and the fit: the slope of the linear fit represents the strength of the mean upwelling conditions and the difference reflects the changes in the intensity of upwelling.

We may follow the procedure in *Castellanos et al*. [2013b] but retaining the $(\rho f)^{-1}$ factor such that the time-integrated cross-shore transport has units of offshore volume per unit length (m^2). Specifically, we redefine the wind impulse to be

$$I(y,t) \equiv \frac{1}{\rho f}\int_0^t \tau_{sy}(y,t')dt', \tag{11}$$

and calculate the wind-impulse anomaly simply as the wind impulse less a linearly changing wind impulse value, $\bar{I}$, as follows

$$\delta I \equiv I-\bar{I}=I-\frac{\bar{\tau}_{sy}t}{\rho f}, \tag{12}$$

where $\bar{\tau}_{sy}$ is the mean alongshore wind stress over the whole available time series.

The wind-impulse anomaly examines the departures from some mean condition (the mean slope of the wind impulse) in order to characterize conditions of enhanced or reduced upwelling. These anomalies actually are an annually detrended time integration of the wind stress which carries a temporal memory at seasonal and shorter time scales, e.g., an anomaly will remain positive during some time despite the wind falls below its mean value. In last section, we argued that this relatively long spatial memory of upwelling arises through the upstream alongshore flow; equation (6) indeed shows that the wind impulse may drive the alongshore velocity of a material water parcel.

We may propose an alternative nonlocal or cumulative index which also takes into consideration the time history of the alongshore winds but in such a way that it searches for the maximum cross correlation between the cumulative index and the actual SST difference. Specifically, we define a time-lagged Ekman transport as

$$CU(y,t)=\frac{1}{\rho f T}\int_{t-T}^{t} \tau_{sy}(y,t')dt', \tag{13}$$

where T represents a time lag (constant for each latitude) that leads to the maximum cross correlation between the seasonal cycle of CU and the seasonal cycle of the SST difference. In this way, we let T be latitude dependent but time independent, implicitly assuming the dynamical processes (responsible for the temporal lag between Ekman transport and SST difference) remain unchanged all year long. Notice that equation (13) reduces to equation (1), i.e., CU becomes U, as the time lag tends to zero.

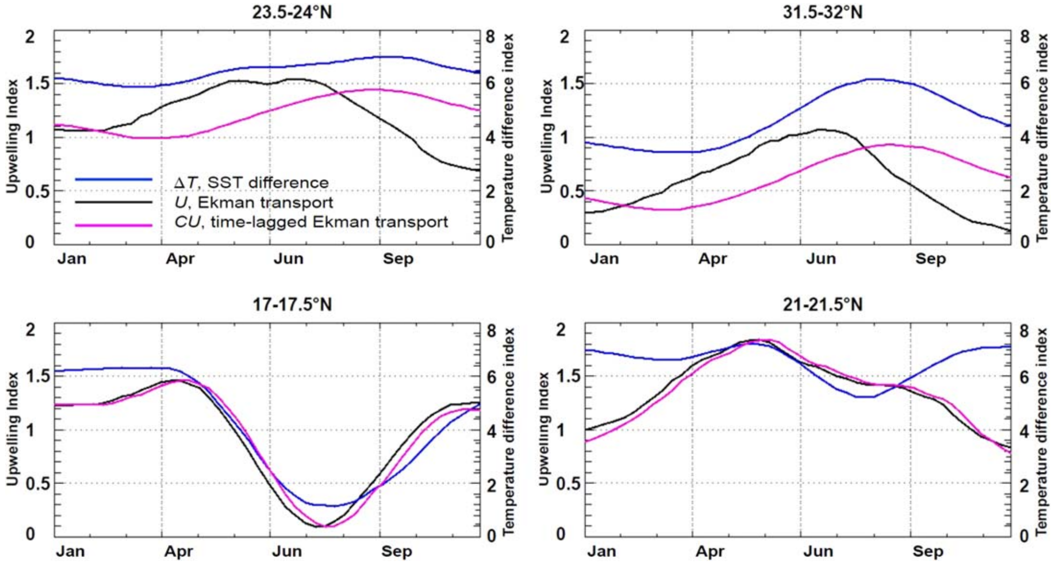

Figure 10. Temperature difference index (°C) as compared with the instantaneous (*U*) and time lagged (*CU*) cross-shore Ekman upwelling indices ($m^2 s^{-1}$), at four different latitudes: (bottom left) 17.5°N, (bottom right) 21.5°N, (top left) 24°N, and (top right) 32°N.

6.2. Time-Latitude Distributions

Let us first illustrate how we calculate the wind-impulse anomaly δI and the cumulative index *CU* at four selected latitudes: 17.5°N, 21.5°N, 24°N, and 32°N. Following *Castellanos et al*. [2013a, 2013b], the impulse is integrated over one full year, starting from zero on 1 January (supporting information Figure S4). In our entire study area, except during the summer months at 17.5°N, the absolute value of the wind impulse increases monotonically with time. The adjustment to the wind impulse, $\bar{I}$, is calculated through a linear fit to a sequence of many consecutive seasonal cycles (usually 10 cycles) (supporting information Figure S4); notice that the slope of this linear adjustment does not intercept the origin and the wind-impulse anomaly is the same at the beginning and end of the annual cycle. The rate of increase is greatest at 21.5°N and 24°N, in the permanent upwelling area between Cape Blanc and the Canary Islands.

The wind-impulse anomaly is next calculated as the difference between the wind impulse and its linear adjustment (supporting information Figure S4). The maximum anomaly values, both positive and negative, occur at 21.5°N and 24°N: the anomalies are positive during the first semester of the year, peaking in March, and negative in the second semester. At 17.5°N, the positive values take place between September and March, while the negative values occur from April to August.

In order to calculate the cumulative upwelling index *CU*, we consider the time history of the wind. This is done by linearly averaging, backward in time during one full year, the offshore Ekman transport: the cumulative index is the one that provides the highest correlation with the SST difference. In practice, this is done by converting, at each time throughout the year, equation (13) into a summation

$$CU=\frac{1}{\rho f(n+1)}\sum_{i=-n}^{0}\tau_{sy}^{i}, \tag{14}$$

where the *i* superindex stands for the time steps between adjacent wind values (every 8 days) and *n* represents the number of time steps that lead to the maximum cross correlation between the seasonal cycle of *CU* and the seasonal cycle of the SST difference.

Figure 10 illustrates the seasonal cycle in SST difference, Ekman transport (*U*), and time-lagged Ekman transport (*CU*) at four selected latitudes. We find *CU* to be very similar to *U* at 17.5°N and 21.5°N (south of and close to Cape Blanc) and substantially different at 24°N and 32°N. In particular, at 32°N, the shape of *CU* is very close to the shape of the SST difference, therefore, representing a correlation that is very close to one.

Figure 11 presents the results of this calculation for all latitudes, illustrating how the simple linear backward average can substantially increase the correlation in many locations. The correlation between *U* and the SST

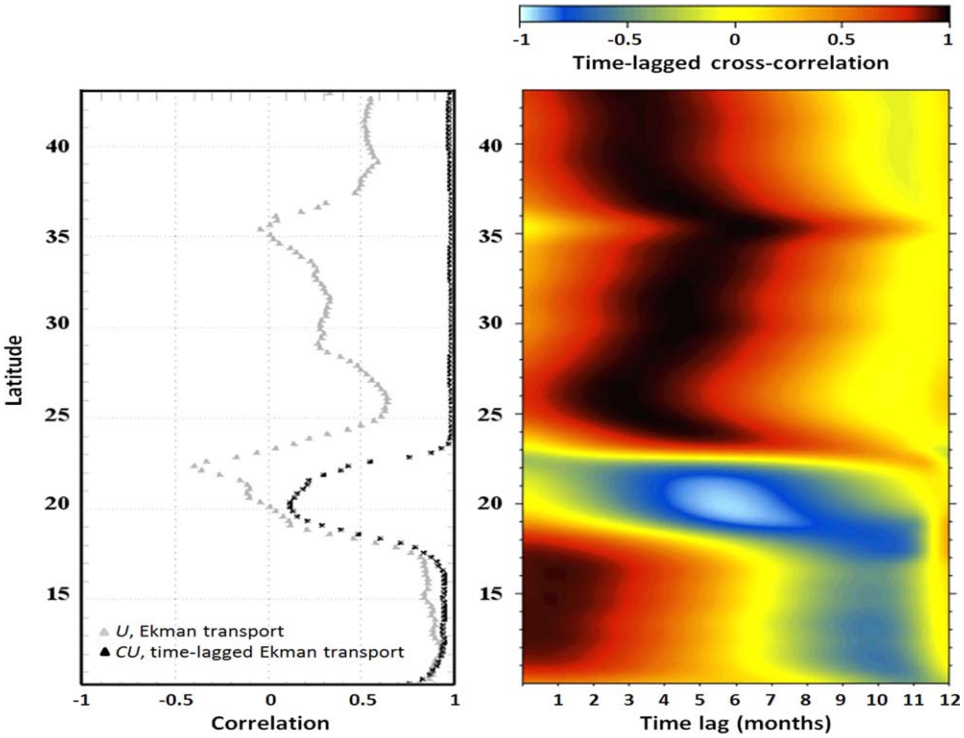

Figure 11. (left) Temporal cross correlation (as a function of latitude) of the temperature difference index with the instantaneous (*U*) and time lagged (*CU*) cross-shore Ekman upwelling indices. (right) Cross correlation between the temperature difference index and the time lagged Ekman upwelling index; the maximum cross correlation sets the value of the cumulative cross-shore Ekman upwelling index (*CU*).

difference is very high (close to 0.9) at latitudes less than 18°N and moderately high (between 0.3 and 0.75) at latitudes from 24°N to 33°N (Figure 11, left). The correlation between *CU* and the SST differences remains, as expected, very large for latitudes less than 18°N and increases greatly, always above 0.9, for latitudes 23°N or higher; only between 18°N and 23°N does the correlation not exceed 0.8, actually falling close to zero near 21°N (Figure 11, right). The time lag for *CU* is close to zero at latitudes less than 23°N (the correlations at zero lag are so high that there is little margin for improvement). At latitudes 23°N or higher the time lag ranges between 8 and 26 weeks, concomitant with the atmosphere-ocean response time scale as inferred from the cross correlations between wind forcing and SST differences (Figure 6, right).

We may finally look at time-latitude plots for these two nonlocal indices (Figure 12), which can be compared with the observed SST difference (Figure 4; in order to ease the comparison the satellite SST difference is reproduced as Figure 12, right). The wind-impulse anomaly shows an antisymmetric pattern, with high values at latitudes less than 18°N during the first semester of the year and high values at latitudes above 18°N during the second semester (Figure 12, left). The calculated pattern does display some similarities with the SST difference but also shows some significant differences: the wind-impulse anomaly, contrarily to the local Ekman index, lags slightly behind the SST difference between 13°N and 18°N, and cannot properly represent times of intermediate conditions, such as those taking place between 20°N and 25°N during the first semester. The cumulative Ekman index, on the other hand, exhibits encouraging similarities with the SST difference in both shape and intensity (Figure 12, middle); the only noticeable distinction is that it overestimates upwelling at low latitudes during the second semester.

The (time) cumulative index represents a significant improvement on the zero-lag cross-shore Ekman transport, endorsing the idea of a coastal upwelling system with temporal memory brought about by the alongshore upwelling jet. We may go one step farther and see if there is also some type of spatial memory, investigating whether the local SST difference is related to the wind stress over a previous period of time and a certain upstream region. Specifically, we compute the upwelling index as in equation (13) but with a double integration, backward in time and alongshore. The resulting time-plus-space cumulative index displays a time-latitude pattern which is very similar to the one for the (solely) time-lagged CU index (Figure 11

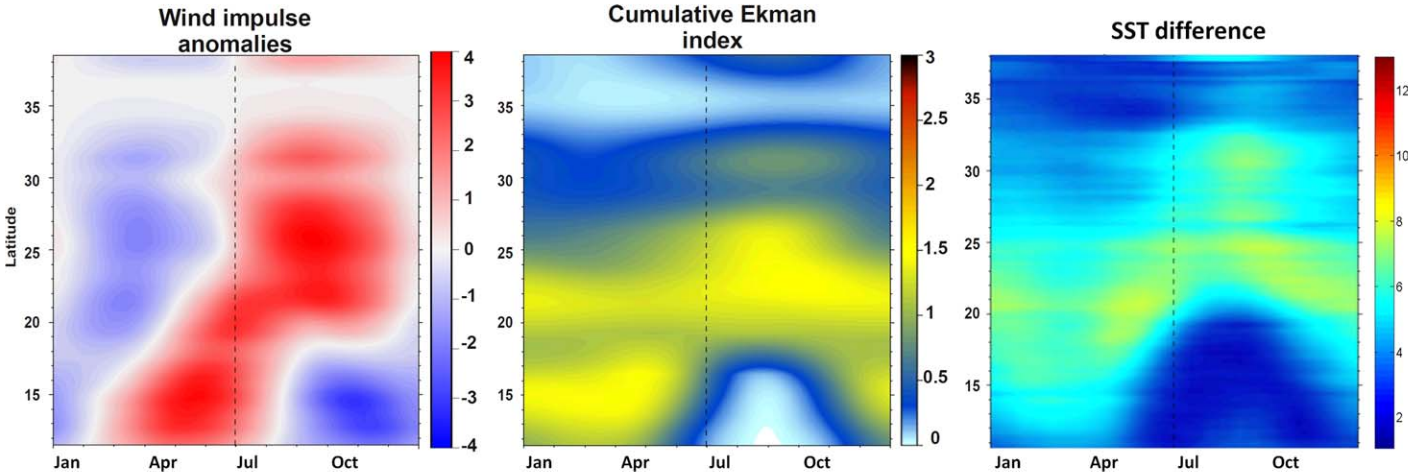

Figure 12. Time-latitude plots of (left) the wind-impulse anomalies (10^6 m^2), (middle) the cumulative cross-shore Ekman upwelling index (m^2 s^{-1}), and (right) the SST difference index as deduced from the 8 day AVHRR data.

and supporting information Figure S5). The level of maximum correlation is essentially unchanged at all latitudes, remaining very close to one, and stays low in the confluence region off Cape Blanc.

Additional information arises when we plot the correlation coefficient as a function of time and distance for several selected latitudes (supporting information Figure S6). The change in the correlation follows a similar pattern whether a function of either time or distance; note the clear seasonality in the correlation, which was already visible in Figure 8. The maximum correlations are found at zero (time and distance) lag south of Cape Blanc and nonzero (temporal and/or spatial) lags north of Cape Blanc. North of Cape Blanc, those lags giving the maximum correlation lie along a line joining the (3–5 months, 0° latitude) and (0 months, 2–3° latitude) points (supporting information Figure S6; distances are to be doubled, as in Figures 7 and 8). Off Cape Blanc (about 21.5°N), in contrast, the correlation remains low independently of the time and spatial lag. We may interpret these results as providing further evidence on the connecting role, both in time and space, played by the alongshore upwelling jet: the spatial and temporal intermittency is smeared out and the upwelling area evolves seasonally, following the annual cycle of the forcing winds.

7. Test Cases: Fall 2007 and 2008

We end up applying the above ideas to two specific years, 2007 and 2008, when we had two extensive fall cruises off NW Africa, i.e., near the end of the upwelling season when there is a significant time lag between the wind and thermal indices. We have two principal objectives: (1) to appreciate how different the conditions can be for one realization as compared with the corresponding mean seasonal situation and (2) to investigate if the nonlocal indices can provide useful information with actual time series data.

In Figure 2, we already appreciated the seasonality of the alongshore winds (CCMP data) at three distinct latitudes (17.5°N, 24°N, and 32°N), with late summer and early fall maximum/minimum values north/south of Cape Blanc (about 21°N); it also became clear that the intermittency increased toward higher latitudes. In Figure 13, we explore the variability of the wind over two 2-month periods (October and November 2007 and 2008), now using the daily QuikSCAT wind data. Again we observe the predominance of upwelling-favorable winds, with only a few short events (1–2 days long) where the winds drop and even reverse, mostly at 32°N.

The spatial distribution of the surface winds, as viewed using two 8 day periods, is illustrated in Figure 14 (top). Winds are generally upwelling favorable, in agreement with the time series at 32°N (Figure 13). The SST fields (Figure 14, bottom) display the existence of generalized low SST coastal values north of Cape Blanc except in the southern Gulf of Cadiz, where the nearshore SST values are not distinctly lower than the offshore values. South of Cape Blanc, upwelling is not evident between 9 and 16 November 2007.

A view of the actual subsurface conditions is possible with the help of the in situ data collected during the 29 October to 20 November 2007 and 3–29 November 2008 cruises (Figure 15 and supporting information Figure S7). The horizontal temperature distributions at 0, 50, 100, and 200 m tell us about the presence and

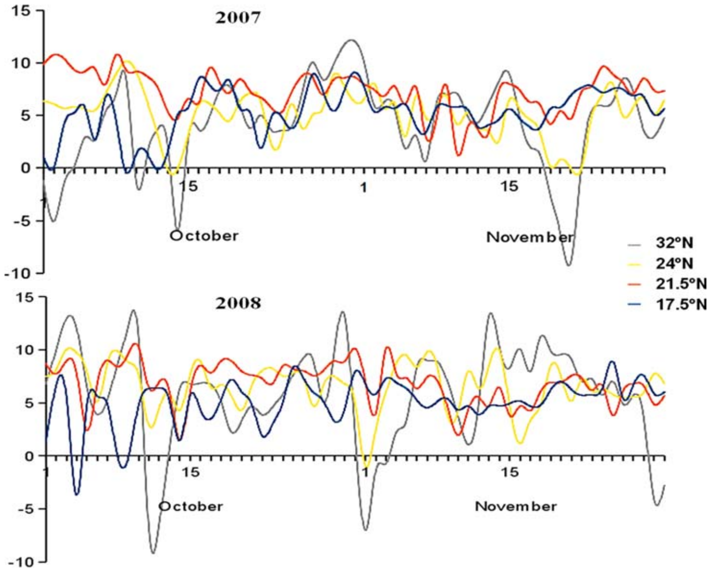

Figure 13. Time series of the alongshore winds (m s^{-1}) at four different latitudes (17.5°N, 21.5°N, 24°N, and 32°N): (top) October-November 2007, (bottom) October-November 2008. The values correspond to a zonal average over 200 km adjacent to the African coastline.

depth of influence of upwelling (Figure 15). We can see that, in agreement with the satellite SST fields, in the southern Gulf of Cadiz and south of Cape Blanc there is little evidence of upwelling at the sea surface; south of Cape Blanc in 2008 (no 2007 data available) and in the southern Gulf of Cadiz in 2007, some weak upwelling signatures can be detected at 50 m and, barely, at 100 m. At a depth of 200 m, upwelling is only apparent north of Cape Blanc. These results are confirmed by the vertical temperature distributions along some selected sections (supporting information Figure S7). The sections along 24°N and 32°N show the presence of very intense upwelling, in 2008 actually extending offshore beyond section 32°N. In contrast, the 34°N section displays a narrow and weak upwelling signal and the 17.5°N section shows a shallow subsurface structure which is suggestive of active upwelling; the weak surface signature at 17.5°N, however, is not always manifest at the sea surface, probably as a result of the rapid heating of the surface tropical waters [*Castellanos et al*., 2013a]. The observations, therefore, indeed reflect the major features present in the climatological fields but also confirm the existence of substantial spatial and temporal intermittency.

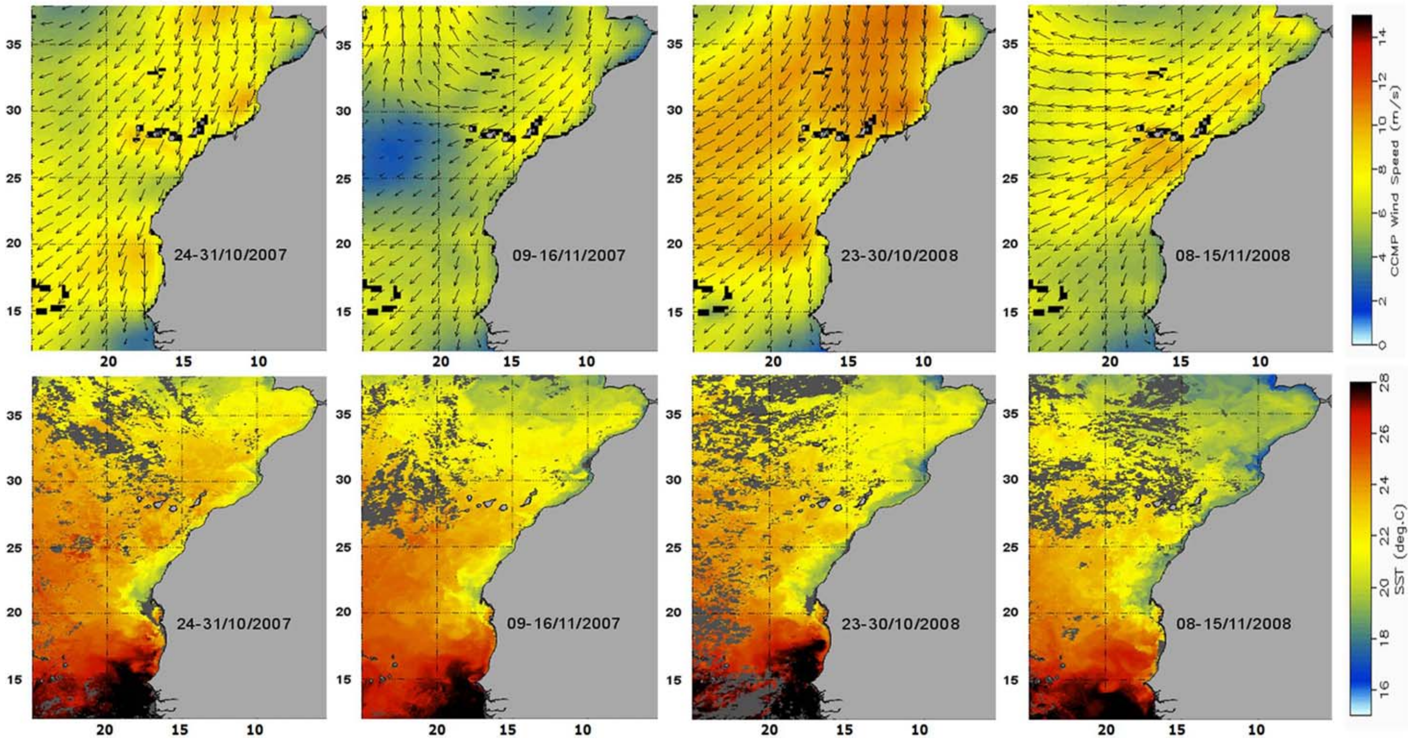

Figure 14. (top) Sea surface winds as obtained from CCMP. (bottom) SST images as obtained from infrared sensors aboard the NOAA satellites. The images correspond to averages over 8 day periods as follows: (column 1) 24–31 October 2007, (column 2) 9–16 November 2007, (column 3) 23–30 October 2008, and (column 4) 8–15 November 2008.

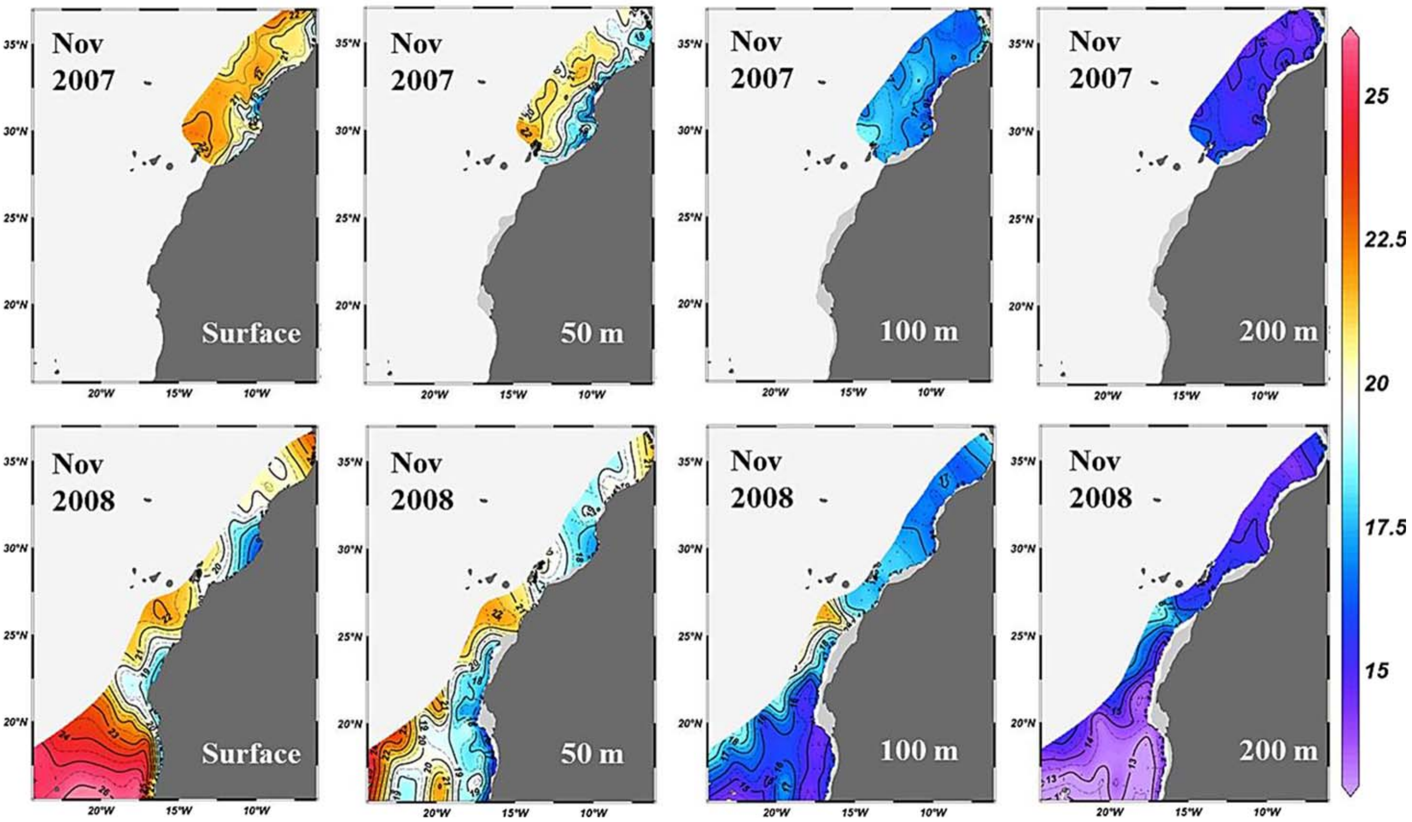

Figure 15. Temperature maps (°C) at (from left to right) 0, 50, 100, and 200 m during November (top) 2007 and (bottom) 2008.

We may calculate the local and nonlocal indices for both years, and see how they fit with the corresponding SST differences. The SST difference does show the same general pattern as for the climatological year, but patchier and with larger peak values (Figure 16, top left), revealing the smoothing effect of climatological averaging; the difference between the two consecutive years is illustrative of the interannual variability which, when averaged, gives rise to the climatological field. The local index, i.e., the cross-shore Ekman transport, has the same general shape as the SST difference but displays some significant differences (Figure 16, top right): relatively strong values at latitudes less than 20°N and a substantial phase lag at latitudes between 21°N and 33°N (SST peak values lagging Ekman transport maxima by about 2 months).

The wind-impulse anomaly, the simplest nonlocal index, is very much in phase with the SST differences at latitudes higher than 26°N but shows only moderate agreement at lower latitudes (Figure 16, bottom left). In particular, in 2007 it completely misses the observed upwelling at these low latitudes during the first semester of the year; in contrast, it has the skill to reasonably well reflect (at least down to 17°N) the weak upwelling that took place in March and April 2008.

The *CU* index closely follows the time-space patterns of the SST differences, i.e., the presence and timing of upwelling is indeed very well reproduced (Figure 16, bottom right). Its major deficiency, however, is that it predicts upwelling to be stronger at low latitudes than high latitudes, the change in regime taking place near Cape Blanc (about 21.5°N). This is because *CU* has very little temporal smoothing at latitudes less than 21.5°N, reproducing the classical Ekman transport very closely, while it is substantial smoothed (typically about 2 months) at latitudes higher than 21.5°N, which reduces the intensity of the peak signal considerably (Figure 11).

8. Conclusions

We have examined the dynamics of coastal upwelling off NW Africa through the seasonality in sea-surface wind forcing and SST response. Conceptual and numerical models tell us that, locally, the sea surface responds very rapidly to wind, on time scales from hours to a few days. Therefore, we could possibly expect

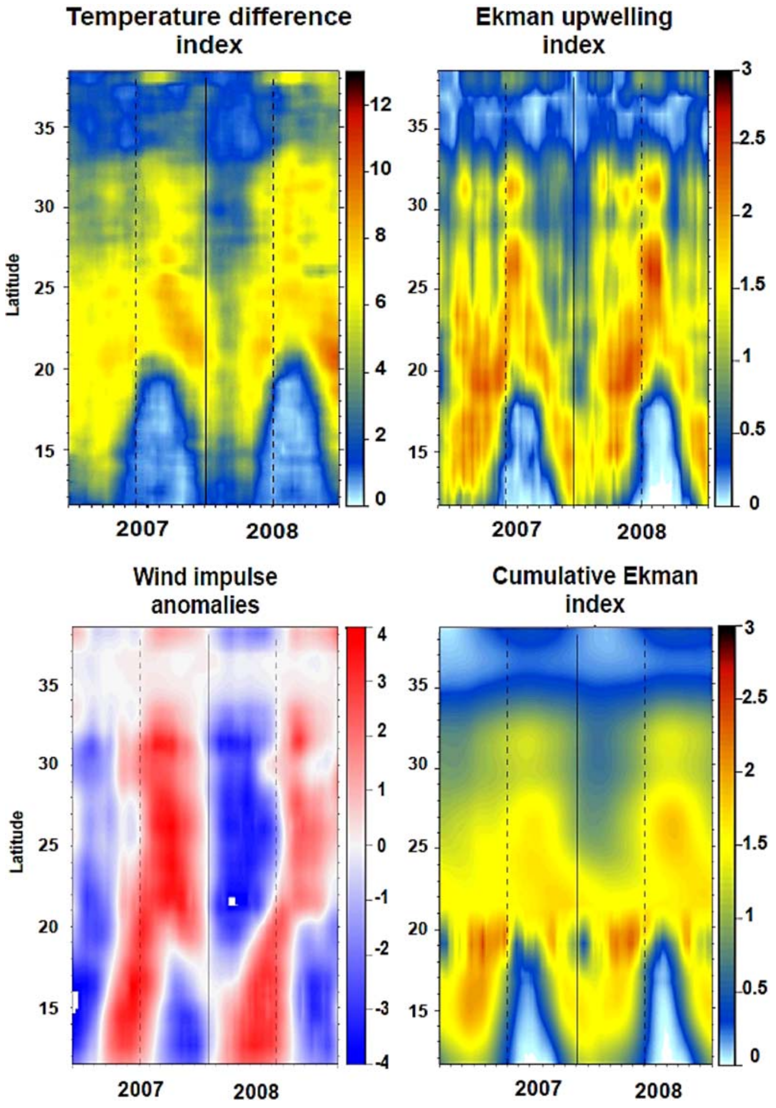

Figure 16. Time-latitude plots of (top left) temperature difference index (°C), (top right) cross-shore Ekman upwelling index ($m^2\ s^{-1}$), (bottom left) wind-impulse anomalies ($10^6\ m^2$), and (bottom right) cumulative cross-shore Ekman upwelling index ($m^2\ s^{-1}$) for the 2007–2008 period.

that the SST difference (between the coast and far offshore) would closely follow the wind forcing, with substantial intermittency at the same weekly time scales as the wind; if this was the case the seasonal cycle would have little predictive value for coastal upwelling. However, our analysis of spatial and temporal correlations shows that the time scales for the ocean response are substantially longer than the wind time scales. This is because of the spatial memory of the upwelling system, which takes place through alongshore advection between adjacent upwelling areas and turns into a relatively long temporal memory. Consequently, the entire upwelling region marches in unison, responding to the seasonal evolution of the forcing winds. When we average the SST-difference values over many years we are effectively removing the signal associated with the short-time changing winds and are left with the dominant regional response, hence the relevance of the climatological cycle.

An analysis of the size of the different terms in the alongshore momentum balance proves the potential relevance of the alongshore momentum advection. We have shown that, in dynamically connected adjacent coastal regions, this advection of momentum is large enough to counteract the role of alongshore internal friction for periods of 2–3 weeks and over distances of order 300 km. These scales are longer than the temporal autocorrelation of the wind (which characterizes the intermittency of the wind) and greater than the alongshore autocorrelation of the SST (which typifies the coherence of the upwelling system) therefore leading to the sustainment of the alongshore baroclinic jet and the associated frontal system. In other words, for the upwelling system to significantly relax it would require the wind to cease for a period longer than 2–3 weeks over distances longer than 300 km; such a widespread arrest is almost never observed off NW Africa for latitudes between Cape Blanc and the Strait of Gibraltar. Rather, the northeasterly winds drive upwelling during periods of the order of 10 days and then relax; two adjacent areas, however, will typically not experience the upwelling-favorable winds simultaneously, so the wind may weaken in an area while it remains upwelling favorable further upstream. The connection takes place through the upwelling baroclinic jet, further enhanced by the nearshore recirculation of the whole eastern boundary system [*Pelegrí et al*., 2005a, 2006], this being the basis for the Canary Upwelling Current (CUC).

The relatively long temporal memory of the system limits the appropriateness of local indices, based solely on local and instantaneous wind forcing, to predict the state of the upper ocean. In this work we have explored the utilization of two different nonlocal indices, both based on the time history of the wind at each location. The implicit assumption is that they reflect the joint effect of local and nonlocal winds, the latter through alongshore advection from adjacent coastal regions which typically do not have very different wind regimes. We have shown that one of these indices, the cumulative Ekman transport, or cumulative index *CU*, does very well at reproducing the shape and timing of upwelling north of Cape Blanc, at the expense of weakening the intensity of peaks through temporal smoothing. The typical time period for the cumulative index in this region ranges between 2 and 4 months, essentially an entire season; this is because of the way we have defined the *CU* index, as an integration over a given lag period.

Some of these ideas do not apply to the area south of Cape Blanc: the latitudinal dynamical connection is substantially reduced because of the northward Mauritania Current. Further, the winds have relatively long temporal memory and short spatial correlations. The result is a very short time lag for the *CU* index, i.e., the Ekman transport (*CU* at lag zero) already does well at predicting the SST difference.

In our study, we have not really looked at interannual variability, except for a short discussion of the similarities and differences between two consecutive years (2007 and 2008), when we had some extensive fall in situ measurements. These 2 years display the same seasonal pattern yet with noticeable differences. We expect that most of the differences arise because of changes in remote forcing mechanisms, affecting the Azores High and the response of the eastern boundary system, such as the El Niño-Southern Oscillation and the North Atlantic Oscillation at interannual scales, and the Atlantic Meridional Mode at interdecadal scales [*Pastor et al*., 2013].

A corollary from our work is the importance of connections between adjacent coastal regions and between the coastal and offshore oceans. Our skill at predicting the evolution of the coastal ocean will remain, in most cases, very limited unless we know how these different areas are interconnected. Under this perspective, future research needs to focus, first, on understanding and assessing the connections, and, second, on building composite indices that include the different spatial and temporal scales.

Acknowledgments
We are very grateful to our three reviewers for many useful and constructive comments and suggestions, which have helped improve the final version of this article. This work has been supported by project TIC-MOC (CTM2011–28867) of the Spanish Ministerio de Ciencia e Innovación. Partial funding from the Institut de Recherche pour le Développement, UMR EME 212, is also gratefully acknowledged. Aïssa Benazzouz was partially supported by the 50th Anniversary Young African fellowship program of the Intergovernmental Oceanographic Commission. Evan Mason was supported by a Spanish government JAE-Doc grant (CSIC), cofinanced by FSE. Jesus Peña-Izquierdo was funded through a FPI doctoral grant linked to project MOC2 (CTM2008-06438-C02-01) of the Spanish Ministerio de Ciencia e Innovación. The SST data were provided by GHRSST and the U.S. National Oceanographic Data Center, in a project partly supported by the NOAA Climate Data Record (CDR). QuikSCAT and CCMP global wind were obtained from the NASA Physical Oceanography Distributed Active Archive Center at the Jet Propulsion Laboratory. ROMS development at UCLA is supported by the Office of Naval Research (currently grant N00014-08-1–0597), the applications here shown were partially supported by the National Center for Supercomputing Applications under grant OCE030007 and utilized the ABE system.

References

Atlas, R., R. N. Hoffman, J. Ardizzone, S. M. Leidner, J. C. Jusem, D. K. Smith, and D. A. Gombos (2011), A cross-calibrated, multiplatform ocean surface wind velocity product for meteorological and oceanographic applications, *Bull. Am. Meteorol. Soc.*, *92*, 157–174.

Bakun, A. (1973), Coastal upwelling indices, west coast of North America, 1946–1971, *NOAA Tech. Rep. NMFS–SSRF–671*, 103 pp., U.S. Dep. of Commer., Seattle, Wash.

Barton, E. D. (1998), Eastern boundary of the North Atlantic: North-west Africa and Iberia, in *The Sea*, edited by A. R. Robinson and K. H. Brink, pp. 633–657, John Wiley, N. Y.

Benazzouz, A., K. Hilmi, A. Orbi, H. Demarcq, and A. Attilah (2006), Dynamique spatio-temporelle de l'upwelling côtier Marocain par tèlèdétection de 1985 à 2005, *Geo Obs.*, *15*, 15–23.

Benazzouz, A., S. Mordane, A. Orbi, M. Chagdali, K. Hilmi, A. Atillah, J. L. Pelegrí, and H. Demarcq (2014), An improved coastal upwelling index from sea surface temperature using satellite-based approach—The case of the Canary Current upwelling system, *Cont. Shelf Res.*, *81*, 38–54.

Carr, M., and E. Kearns (2003), Production regimes in four Boundary Current Systems, *Deep Sea Res., Part II*, *50*, 3199–3221.

Castellanos, P., J. L. Pelegrí, D. Baldwin, W. J. Emery, and A. Hernández-Guerra (2013a), Winter and spring surface velocity fields in the Cape Blanc region as deduced with the Maximum Cross-Correlation technique, *Int. J. Remote Sens.*, *34*, 3587–3606.

Castellanos, P., J. L. Pelegrí, and A. Benazzouz (2013b), Wind-driven surface circulation in the Cape Blanc region, *Cont. Shelf Res.*, *60*, 87–103.

Choboter, P. F., D. Duke, J. P. Horton, and P. Sinz (2011), Exact solutions of wind-driven coastal upwelling and downwelling over sloping topography, *J. Phys. Oceanogr.*, *41*, 1277–1296.

Csanady, G. T. (1977), Intermittent "full" upwelling in Lake Ontario, *J. Geophys. Res.*, *82*, 397–419.

Csanady, G. T. (1982), *Circulation in the Coastal Ocean*, D. Reidel. Pub., 279 pp., Chichester, U. K.

Demarcq, H., and E. V. Faure (2000), Coastal upwelling and associated retention indices derived from satellite SST: Application to Octopus vulgaris recruitment, *Oceanol. Acta*, *4*, 11231–11246.

DeSzoeke, A., and J. G. Richman (1981), The role of wind generated mixing in coastal upwelling, *J. Phys. Oceanogr.*, *11*, 1534–1547.

DeSzoeke, A., and J. G. Richman (1984), On wind-driven mixed layers with strong horizontal gradients—A theory with application to coastal upwelling, *J. Phys. Oceanogr.*, *14*, 364–377.

Ekman, V. W. (1905), On the influence of the Earth's rotation on ocean-currents, *Ark. Mat. Astron. Fys.*, *2*, 1–52.

Estrade, P., P. Marchesiello, A. C. De Verdiere, and C. Roy (2008), Cross-shelf structure of coastal upwelling: A two-dimensional extension of Ekman's theory and a mechanism for inner shelf upwelling shut down, *J. Mar. Res.*, *66*, 589–616.

Gabric, A. J., L. García, L. VanCamp, L. Nykjaer, W. Eiffer, and W. Schrimpf (1993), Offshore export of shelf production in the Cape Blanc (Mauritania) giant filament as derived from coastal zone color scanner imagery, *J. Geophys. Res.*, *98*, 4697–4712.

Geisler, J. E., and E. B. Kraus (1969), The well-mixed Ekman boundary layer, *Deep Sea Res. Oceanogr. Abstr.*, *14*, suppl., 73–84.

Gill, A. E. (1982), *Atmosphere–Ocean Dynamics*, 662 pp., Academic, N. Y.

Gill, A. E., and A. J. Clarke (1974), Wind-induced upwelling, coasal corrents and sea-level changes, *Deep Sea Res.*, *21*, 325–345.

Hempel, G. (Ed.) (1982), The Canary Current: Studies of an Upwelling System, *Rapp. P. V. Réun. Cons. Int. Explor. Mer*, *180*, 455.

Hernández-Guerra, A., and L. Nykjaer (1997), Sea surface temperature variability off northwest Africa: 1981–1989, *Int. J. Remote Sens.*, *18*, 2539–2558.

Kundu, P. K., and R. C. Beardsley (1991), Evidence of a critical Richardson number in moored measurements during the upwelling season off Northern California, *J. Geophys. Res.*, *96*, 4855–4868.

Laiz, I., J. L. Pelegrí, F. Machín, P. Sangrà, A. Hernández-Guerra, A. Marrero-Díaz, and A. Rodríguez-Santana (2012), Eastern boundary drainage of the North Atlantic subtropical gyre, *Ocean Dyn.*, *62*, 1287–1310.

Lazaro, C., M. Fernandes, A. M. P. Santos, and P. Oliveira (2005), Seasonal and interannual variability of surface circulation in the Cape Verde region from 8 years of merged T/P and ERS-2 altimeter data, *Remote Sens. Environ.*, *98*, 45–62.

Lee, S. K., J. L. Pelegrí, and J. Kroll (2001), Slope control in western boundary currents, *J. Phys. Oceanogr.*, *31*, 3349–3360.

Lentz, S. J., and D. C. Chapman (2004), The importance of nonlinear cross-shelf momentum flux during wind-driven coastal upwelling, *J. Phys. Oceanogr.*, *34*, 2444–2457.

Machín, F., A. Hernández-Guerra, and J. L. Pelegrí (2006), Mass fluxes in the Canary Basin, *Prog. Oceanogr.*, *70*, 416–447.

Marcello, J., A. Hernández-Guerra, F. Eugenio, and A. Fonte (2011), Seasonal and temporal study northwest African upwelling System, *Int. J. Remote Sens.*, *32*, 1843–1859.

Marchesiello, P., and P. Estrade (2010), Upwelling limitation by onshore geostrophic flow, *J. Mar. Res.*, *68*, 37–42.

Mason, E., F. Colas, J. Molemaker, A. F. Shchepetkin, C. Troupin, J. C. McWilliams, and P. Sangrà (2011), Seasonal variability of the Canary Current: A numerical study, *J. Geophys. Res.*, *116*, C06001, doi:10.1029/2010JC006665.

Mason, E., F. Colas, and J. L. Pelegrí (2012), Origin and fate of upwelled waters in the Canary coastal transition zone, *Sci. Mar.*, *76*(S1), 79–94.

Mittelstaedt, E. (1983), The upwelling area off Northwest Africa: A description of phenomena related to coastal upwelling, *Prog. Oceanogr.*, *12*, 307–331.

Mittelstaedt, E. (1991), The ocean boundary along the Northwest African coast: Circulation and oceanographic properties at the sea surface, *Prog. Oceanogr.*, *26*, 307–355.

Nykjaer, L., and L. VanCamp (1994), Seasonal and interanual variability of coastal upwelling along northwest Africa and Portugal from 1981 to 1991, *J. Geophys. Res.*, *99*, 14,197–14,207.

Pardo, P., X. Padín, M. Gilcoto, L. Fariña-Busto, and F. Pérez (2011), Evolution of upwelling systems coupled to the long-term variability in sea surface temperature and Ekman transport, *Clim. Res.*, *48*, 231–246.

Pastor, M. V., J. L. Pelegrí, A. Hernández-Guerra, J. Font, J. Salat, and M. Emelianov (2008), Water and nutrient fluxes off northwest Africa, *Cont. Shelf Res.*, *28*, 915–936.

Pastor, M. V., J. Peña-Izquierdo, J. L. Pelegrí, and A. Marrero-Díaz (2012), Meridional changes in water properties off NW during November 2007/2008, *Cienc. Mar.*, *38*(1B), 223–244.

Pastor, M. V., J. B. Palter, J. L. Pelegrí, and J. P. Dunne (2013), Physical drivers of interannual chlorophyll variability in the eastern subtropical North Atlantic, *J. Geophys. Res. Oceans*, *118*, 3871–3886, doi:10.1002/jgrc.20254.

Pelegrí, J. L., and J. G. Richman (1993), On the role of shear mixing during transient coastal upwelling, *Cont. Shelf Res.*, *13*, 1363–1400.

Pelegrí, J. L., J. Arístegui, L. Cana, M. González, A. Hernández-Guerra, S. Hernández-León, A. Marrero-Díaz, M. F. Montero, P. Sangrá, and M. Santana-Casiano (2005a), Coupling between the open ocean and the coastal upwelling region off Northwest Africa: Water recirculation and offshore pumping of organic matter, *J. Mar. Syst.*, *54*, 3–37.

Pelegrí, J. L., et al. (2005b), Hydrographic cruises off northwest Africa: The Canary Current and the Cape Ghir region, *J. Mar. Syst.*, *54*, 39–63.

Pelegrí, J. L., A. Marrero-Díaz, and A. W. Ratsimandresy (2006), Nutrient irrigation of the North Atlantic, *Prog. Oceanogr.*, *70*, 366–406.

Peña-Izquierdo, J., J. L. Pelegrí, M. V. Pastor, P. Castellanos, M. Emelianov, J. Salvador, and E. Vázquez-Domínguez (2012), The continental slope current system between Cape Verde and the Canary Islands, *Sci. Mar.*, *76*(S1), 65–78.

Peters, H., M. C. Gregg, and J. M. Toole (1988), On the parameterization of equatorial turbulence, *J. Geophys. Res.*, *93*, 1199–1218.

Pierce, S. D., J. A. Barth, R. E. Thomas, and G. W. Fleischer (2006), Anomalously warm July 2005 in the northern California Current: Historical context and the significance of cumulative wind stress, *Geophys. Res. Lett.*, *33*, L22S04, doi:10.1029/2006GL027149.

Ratsimandresy, A. W., J. L. Pelegrí, A. Marrero-Díaz, A. Hernández-Guerra, A. Antoranz, and A. Martínez (2001), Seasonal variability of the upper warmwatersphere in the Canary Basin, *Sci. Mar.*, *65*(S1), 251–258.

Risien, C. M., and D. B. Chelton (2008), A global climatology of surface wind and wind stress fields from eight years of QuikSCAT scatterometer data, *J. Phys. Oceanogr.*, *38*, 2379–2413.

Ruiz, S., J. L. Pelegrí, M. Emelianov, A. Pascual, and E. Mason (2014), Geostrophic and ageostrophic circulation of a shallow anticyclonic eddy off Cape Bojador, *J. Geophys. Res. Oceans*, *119*, 1258–1270, doi:10.1002/2013JC009169.

Samelson, R. M., and R. A. DeSzoeke (1988), Semigeostrophic wind-driven thermocline upwelling at a coastal boundary, *J. Phys. Oceanogr.*, *18*, 1372–1383.

Sangrà, P., et al. (2009), The Canary Eddy Corridor: A major pathway for long-lived eddies in the North Atlantic, *Deep Sea Res., Part I*, *56*, 2100–2114.

Santos, M. P., A. S. Kazmin, and A. Peliz (2005), Decadal changes in the Canary upwelling system as revealed by satellite observations: Their impact on productivity, *J. Mar. Res.*, *63*, 359–379.

Schwing, F. B., N. A. Bond, S. J. Bograd, T. Mitchell, M. A. Alexander, and N. Mantua (2006), Delayed coastal upwelling along the U.S. West Coast in 2005: A historical perspective, *Geophys. Res. Lett.*, *33*, L22S01, doi:10.1029/2006GL026911.

Shchepetkin, A. F., and J. C. McWilliams (2005), The Regional Oceanic Modeling System (ROMS): A split-explicit, free-surface, topography-following-coordinate oceanic model, *Ocean Modell.*, *9*, 347–404.

Speth, P., H. Detlefsen, and H. W. Sierts (1978), Meteorological influence on upwelling off Northwest Africa, *Dtsch. Hydrogr. Z.*, *31*, 95–104.

Trenberth, K. E., W. G. Large, and J. G. Olson (1990), The mean anual cycle in global ocean wind stress, *J. Phys. Oceanogr.*, *20*, 1742–1760.

Troupin, C., F. Machín, M. Ouberdous, D. Sirjacobs, A. Barth, and J. M. Beckers (2010), High-resolution climatology of the northeast Atlantic using Data-Interpolating Variational Analysis (Diva), *J. Geophys. Res.*, *115*, C08005, doi:10.1029/2009JC005512.

Van Camp, L., L. Nykjaer, E. Mittelstaedt, and P. Schlittenhardt (1991), Upwelling and boundary circulation off Northwest Africa as depicted by infrared and visible satellite observations, *Prog. Oceanogr.*, *26*, 357–402.

Wooster, W. S., A. Bakun, and D. R. McLain (1976), The seasonal upwelling cycle along the eastern boundary of the North Atlantic, *J. Mar. Res.*, *34*, 131–141.